

1 From ether to acid: a plausible degradation pathway of glycerol
2 dialkyl glycerol tetraethers

3

4 Xiao-Lei Liu ^{a,b,*}, Daniel Birgel ^c, Felix J. Elling ^{a,#}, Paul A. Sutton ^d, Julius S. Lipp ^a,
5 Rong Zhu ^{a,§}, Chuanlun Zhang ^e, Martin Könneke ^a, Jörn Peckmann ^{c,f}, Steven J.
6 Rowland ^d, Roger E. Summons ^b, Kai-Uwe Hinrichs ^a

7

8

9 ^a Organic Geochemistry Group, MARUM Center for Marine Environmental Sciences and
10 Department of Geosciences, University of Bremen, 28359 Bremen, Germany

11 ^b Department of Earth, Atmospheric, and Planetary Sciences, Massachusetts Institute of
12 Technology, 77 Massachusetts Avenue, Cambridge, MA 02139-4307, USA

13 ^c Institute of Geology, University of Hamburg, 20146 Hamburg, Germany

14 ^d School of Geography, Earth and Environmental Sciences, University of Plymouth,
15 Plymouth, Devon PL4 8AA, U.K.

16 ^e State Key Laboratory of Marine Geology, Tongji University, Shanghai 200092, China

17 ^f Department of Geodynamics and Sedimentology, Center for Earth Sciences, University
18 of Vienna, 1090 Vienna, Austria

19 [#] Present address, Harvard University, 20 Oxford St, Cambridge, MA 02138, USA

20 [§] Present address, ETH Zurich, Universitätsstrasse 16, 8092 Zürich, Switzerland

21

22 * Corresponding author, E-mail: xlliu@mit.edu

23

24

25 **Abstract**

26

27 Glycerol dialkyl glycerol tetraethers (GDGTs) are ubiquitous microbial lipids with
28 extensive demonstrated and potential roles as paleoenvironmental proxies. Despite the
29 great attention they receive, comparatively little is known regarding their diagenetic fate.
30 Putative degradation products of GDGTs, identified as hydroxyl and carboxyl derivatives,
31 were detected in lipid extracts of marine sediment, seep carbonate, hot spring sediment
32 and cells of the marine thaumarchaeon *Nitrosopumilus maritimus*. The distribution of
33 GDGT degradation products in environmental samples suggests that both biotic and
34 abiotic processes act as sinks for GDGTs. More than a hundred newly recognized
35 degradation products afford a view of the stepwise degradation of GDGT via 1) ether
36 bond hydrolysis yielding hydroxyl isoprenoids, namely, GDGTol (glycerol dialkyl
37 glycerol triether alcohol), GMGD (glycerol monobiphytanyl glycerol diether), GDD
38 (glycerol dibiphytanol diether), GMM (glycerol monobiphytanol monoether) and bpdioI
39 (biphytanic diol); 2) oxidation of isoprenoidal alcohols into corresponding carboxyl
40 derivatives and 3) chain shortening to yield C₃₉ and smaller isoprenoids. This plausible
41 GDGT degradation pathway from glycerol ethers to isoprenoidal fatty acids provides the
42 link to commonly detected head-to-head linked long chain isoprenoidal hydrocarbons in
43 petroleum and sediment samples. The problematic C₈₀ to C₈₂ tetraacids that cause
44 naphthenate deposits in some oil production facilities can be generated from H-shaped
45 glycerol monoalkyl glycerol tetraethers (GMGTs) following the same process, as
46 indicated by the distribution of related derivatives in hydrothermally influenced
47 sediments.

48

49 **1. INTRODUCTION**

50

51 Lipid biomarkers have the potential of providing valuable information regarding the
52 composition of ancient ecosystems and paleoenvironmental conditions throughout most
53 of the sedimentary record (e.g., Peters et al., 2004). For most of the frequently used
54 biomarkers, such as steroids, hopanoids, pigments and their derivatives, the post-
55 depositional structural transformations are rather well constrained (e.g., Mackenzie et al.,
56 1982; Innes et al., 1997; Peters et al., 2004; Brocks and Schaeffer, 2008) and contribute
57 to the foundation of the geological biomarker concept that links geomolecules to their
58 biological precursors. An exception is the intensively studied group of isoprenoidal
59 glycerol dialkyl glycerol tetraether (GDGT) lipids produced by Archaea. Despite their
60 prominent use as molecular proxies for the reconstruction of paleoenvironmental
61 conditions (e.g., Pearson and Ingalls, 2013; Schouten et al., 2013) and, in their intact
62 polar form, for the ecology of extant archaeal communities (e.g., Lipp and Hinrichs, 2009;
63 Liu et al., 2011; Meador et al., 2015; Yoshinaga et al., 2015), our understanding of their
64 post-depositional behavior is fragmentary.

65

66 Three principal archaeal lipid categories are observed in environmental and geological
67 samples: (i) intact polar lipids (IPL) as building blocks of the cellular membrane,
68 consisting of a glycerolalkylether backbone and a polar headgroup which, in most
69 instances, is glycosidic (Sturt et al., 2004, Lipp and Hinrichs, 2009), (ii) the
70 corresponding core glycerol alkyl ethers derived from hydrolytic cleavage of the polar
71 headgroups on timescales of days to several tens of millennia, depending on depositional

72 conditions and enzymatic activity (Harvey et al., 1986; Xie et al., 2013), and (iii)
73 degradation products of core glycerol alkyl ethers that occur as hydrocarbons (Moldowan
74 and Seifert, 1979), alcohols (Schouten et al., 1998; Saito and Suzuki, 2010) and
75 carboxylic acids (Meunier-Christmann, 1988; Schouten et al., 2003; Birgel et al., 2008a).

76

77 The second group, i.e., the core lipids, is among the most extensively studied biomarker
78 class in the last decade (Pearson and Ingalls, 2013; Schouten et al., 2013), in particular
79 the GDGT derivatives. More than thirty years ago Chappe et al. (1982) had reported the
80 widespread presence of glycerol di- and tetraethers in sediments and petroleum. GDGTs
81 accumulate in cold and moderately heated aquatic sediments with seemingly little
82 molecular alteration and remain intact in sediments over tens of millions of years (e.g.,
83 Kuypers et al., 2001). GDGTs, including the bacterial non-isoprenoidal types (Weijers et
84 al., 2006; Liu et al., 2012b), are among the most prominent lipids in marine sediments
85 and soils. Their ubiquity and abundance result from both the widespread distribution of
86 their producing, largely uncultured, microbes and their relatively high recalcitrance
87 caused by the ether-linkages. Within the domain Archaea, GDGTs are taxonomically
88 widely distributed and probably produced by members of all phyla (Pearson and Ingalls,
89 2013; Schouten et al., 2013).

90

91 Thermal diagenesis (Rowland, 1990) and hydrous pyrolysis (Pease et al., 1998)
92 experiments have shown the generation of isoprenoidal hydrocarbons from fresh archaeal
93 cultures. The exact fate of GDGTs is not clear, but they seem to be the most plausible
94 precursors of a wealth of compounds of putative archaeal origin found in thermally

95 mature formations. These compounds include head-to-head linked C₃₂ to C₄₀ isoprenoid
96 hydrocarbons in petroleum samples (Moldowan and Seifert, 1979), biphytanic diols
97 (Schouten et al., 1998; Saito and Suzuki, 2010) and biphytanic diacids (Meunier-
98 Christmann, 1988; Birgel et al., 2008a) in recent sediments and rock samples of possibly
99 diagenetic and/or biogenic origin; however these diols or diacids have never been
100 detected in any archaeal cell extracts. Another group of recently discovered, widespread
101 compounds includes a series of glycerol ether derivatives, the glycerol dibiphytanol
102 diethers (GDDs; Knappy and Keely, 2012; Liu et al., 2012a). Although the occurrence of
103 core GDDs and their glycosidic intact polar lipids in archaeal cell extracts suggests that
104 they play a role in archaeal lipid biosynthesis (Liu et al., 2012a; Meador et al., 2014), a
105 diagenetic contribution of these lipids in natural settings cannot be ruled out (e.g., Yang
106 et al., 2014).

107

108 Another conspicuous compound series of putative archaeal origin are the so-called ‘H-
109 shaped’ or ‘ARN’ C₈₀-C₈₂ isoprenoidal tetracarboxylic acids found in certain petroleum
110 types (Lutnaes et al., 2006, 2007) and believed to contribute significantly to the
111 problematic naphthenate deposits formed during oil processing (e.g., Baugh et al., 2004;
112 2005). The archaeal lipids that are structurally related to the C₈₀ tetraacids are ‘H-shaped’
113 glycerol monoalkyl glycerol tetraethers (H-GMGTs) found in thermophilic archaeal taxa
114 (Morii et al., 1998; Schouten et al., 2008a), although H-GMGT-0 may also have non-
115 thermophilic origins (Schouten et al. 2013). Whether the C₈₀ tetraacids are degradation
116 products of H-GMGTs or actually bio-surfactants directly synthesized by Archaea living

117 in the crude oil remains ambiguous (Lutnaes et al., 2006, 2007). To date, isoprenoidal
118 tetracarboxylic acids have not been detected in archaeal cells.

119

120 Based on the distribution patterns of newly identified series of GDGT degradation
121 products in sedimentary samples (hydrothermally overprinted sediments from the
122 Guaymas Basin and a hot spring in China, Miocene seep carbonates, and marine
123 subsurface sediments), cell extracts and hydrolysis experiments, here we construct a
124 precursor-product reaction network from GDGTs to alcoholic and carboxylic acid
125 biphytane derivatives. Additionally, through the identification of five types of putative
126 intermediates in the sediment from Guaymas Basin, we provide strong support for the
127 hypothesis that isoprenoidal C₈₀ to C₈₂ tetraacids are derived from step-wise degradation
128 of 'H-shaped' GMGTs.

129

130 **2. MATERIALS and METHODS**

131

132 **2.1. Sample collection and preparation**

133

134 *N. maritimus* strain SCM1 was grown aerobically at 28 °C and pH 7.5 in 8.5 l HEPES-
135 buffered Synthetic Crenarchaeota Medium (1.5 mM NH₄Cl; Könneke et al., 2005;
136 Martens-Habbena et al., 2009). The medium was inoculated with 5% of a mid-
137 logarithmic phase pre-culture of *N. maritimus*. Biomass was harvested early and late in
138 the growth phase as well as early and late in the stationary phase (one batch for each
139 time-point) using cross-flow filtration (Elling et al., 2014). Purity of the culture was

140 checked daily by phase contrast microscopy. Growth was monitored by measuring nitrite
141 formation photometrically (Stickland and Parsons, 1972) and by counting 2%
142 formaldehyde-fixed, SYBR Green I stained cells (Lunau et al., 2005) at the beginning
143 and the end of the experiment. Lipids were extracted from each batch following a
144 modified Bligh and Dyer protocol as described previously (Sturt et al., 2004; Elling et al.,
145 2014).

146

147 The Marmorito seep carbonate samples (Marmorito limestone; see also Peckmann et al.,
148 1999) were taken close to the village of Marmorito, in the Monferrato hills close to
149 Torino, Italy. The Marmorito limestone is composed of dolomite and calcite, and is
150 embedded in Miocene strata chiefly consisting of siliciclastic sediments that were
151 deposited in a marine shelf environment. Rock samples from the vicinity Marmorito,
152 comprising not only the so-called Marmorito limestone, are among the early examples
153 where methane-seepage, fossil chemosynthetic benthic communities, molecular fossils,
154 and methane-related carbonate precipitation have been described (e.g., Clari et al., 1988,
155 1994; Peckmann et al., 1999; Thiel et al., 1999). Apart from the characteristic molecular
156 fossils of the consortium mediating the anaerobic oxidation of methane, biomarkers of
157 aerobic methanotrophic bacteria were also found (Peckmann et al., 1999; Birgel and
158 Peckmann, 2008). A detailed list of compounds identified in the Marmorito limestone
159 and a description of the applied decalcification procedure can be found in Birgel and
160 Peckmann (2008) and references therein. Lipid extraction was performed as described in
161 Birgel et al. (2006).

162

163 The Guaymas Basin sediment sample was retrieved during the *RV Atlantis* cruise AT15-
164 56 to the Guaymas Basin, Gulf of California, Mexico, during *Alvin* dive 4568 (November
165 22 to December 6 2009, 27° 00.449' N, 111° 24.347' W). The sample came from an oil-
166 impregnated hydrothermally active area, where sedimentary temperature steeply
167 increased from ~3 °C to ~100 °C within 35 cm (Gutierrez et al., 2015). The sample was
168 surface sediment (0-4 cm depth) with the highest temperature at time of sampling
169 reaching ~12 °C. However, due to the dynamic nature of the hydrothermal activity and
170 the upward flux of fluids in the Guaymas Basin (Pearson et al., 2005), it is likely that the
171 sample has been previously heated to higher temperatures and/or contains extractable
172 organic matter formed in deeper layers at higher temperatures. Wet sediment (15-20 g)
173 was extracted using the modified Bligh and Dyer method (Sturt et al., 2004). To
174 minimize the heavy background of oil contaminants, an aliquot of the total lipid extract
175 (TLE) was cleaned with the Hybrid SPE[®]-Phospholipid cartridges before LC-MS
176 analysis according to the method described by Zhu et al. (2013a).

177

178 Two further sediment samples, including a marine subsurface sediment (Leg201-1227;
179 Hole 1227A, mixed from five samples: 1227A-2H2-65-75cm, 1227A-2H5-83-93cm,
180 1227A-3H2-55-65cm, 1227A-11H2-118-128m, 1227A-13H3-0-15cm; spanning from
181 8.1-113.6 m below sea floor) and a hot spring sediment (T-15, see sample description in
182 SI) were also extracted with the Bligh and Dyer method for lipid analysis.

183

184 **2.2. Lipid analysis**

185

186 For lipid analysis by normal phase liquid chromatography (NP-LC), an aliquot of TLE of
187 each sample was dissolved in *n*-hexane/isopropanol (99.5:0.5 v/v) for injection.
188 Compound separation was performed on a Dionex Ultimate 3000 RS UHPLC system
189 (Thermo Scientific, Bremen, Germany) at 50 °C, following the recently developed
190 tandem column protocol (Becker et al., 2013) using two ACQUITY UPLC® BEH HILIC
191 Amide columns (2.1 x 150 mm, 1.7 µm, Waters). Solvent gradient was programmed for a
192 constant flow rate of 0.5 mL min⁻¹ and a linear increase from 3% B to 20% B in 20
193 minutes, and then linearly to 50% B at 35 minutes, after then up to 100% B at 45 min,
194 holding for 6 minutes, finally back to 3% B for 9 minutes to re-equilibrate the column,
195 where A was *n*-hexane and B was *n*-hexane/isopropanol (90:10). Detection was achieved
196 with a Bruker Maxis accurate-mass quadrupole time-of-flight (qTOF) mass spectrometer
197 (Bruker Daltonik, Bremen, Germany) coupled to the UHPLC via an atmospheric pressure
198 chemical ionization (APCI) interface run in positive ion mode. APCI source parameters
199 were as follows: corona current 3500 nA, nebulizer gas pressure 5 bar, drying gas flow 8
200 L min⁻¹, drying gas (N₂) temperature 160 °C, vaporizer temperature 400 °C. The scan
201 range was 150-2000 *m/z* at a rate of 2 Hz. Lipids were identified based on accurate mass
202 (better than 1 ppm), retention times and diagnostic fragments and under consideration of
203 general GDGT mass spectral features (e.g., Liu et al., 2012b), and quantified by
204 measurement of [M+H]⁺ responses, with a extraction window of individual ion
205 chromatograms of ± 0.01 *m/z* units.
206
207 For the detection of carboxylic acid derivatives, reversed phase (RP) LC-MS (cf. Zhu et
208 al., 2013b) was applied with the same LC system using an ACE3 C₁₈ column (2.1 × 150

209 mm, 3 μm ; Advanced Chromatography Technologies Ltd., Aberdeen, Scotland) coupled
210 with a guard cartridge and maintained at 45 $^{\circ}\text{C}$, and the same mass spectrometer (qTOF)
211 equipped with an electrospray ionization (ESI) source and operated in positive mode
212 (Bruker Daltonik, Bremen, Germany). An aliquot of TLE of each sample was dissolved
213 in methanol prior to injection. Separation of compounds was achieved isocratically with
214 100% eluent A for 10 min, followed by a rapid gradient to 24% B in 5 min, and then a
215 slow gradient to 65% B in 55 min at a flow rate of 0.2 mL min^{-1} , where the eluent A was
216 methanol/formic acid/14.8 M $\text{NH}_{3\text{aq}}$ (100:0.04:0.10, v/v/v) and B was 2-propanol/formic
217 acid/14.8 M $\text{NH}_{3\text{(aq)}}$ (100:0.04:0.10, v/v/v). After each run, the column was washed with
218 90% B for 10 min and subsequently re-equilibrated with 100% A for another 10 min. The
219 ESI-MS conditions were set as capillary voltage 4500 V, nebulizing gas (N_2) pressure 0.8
220 bar, and dry gas (N_2) 4 L min^{-1} at a temperature of 200 $^{\circ}\text{C}$.

221

222 **3. RESULTS**

223

224 **3.1. Structural elucidation of products of GDGT breakdown**

225

226 Table 1 provides an overview of 19 distinct compound classes observed in this study.
227 Structural assignments are based on formulae established from accurate mass
228 measurements, chromatographic behavior and tandem mass spectrometry (MS^2) (Fig. 1, 2
229 and 3 and S1a-d contain data showing detailed MS^2 fragmentation patterns). Many
230 compounds remain only tentatively identified. Identifications of the hydroxyl derivatives,
231 including GDGTol (glycerol dialkyl glycerol triether alcohol), GMGD (glycerol

232 monobiphytanyl glycerol diether), GDD (glycerol dibiphytanol diether), GMM (glycerol
233 monobiphytanol monoether) and bpdol (biphytanic diol), were additionally confirmed by
234 examination of products released after acidic degradation of purified GDGT-0
235 (compound compositions are given in Fig. S2, and see experiment description in SI). The
236 identification of the H-tetrol was additionally supported by the co-injection of an H-tetrol
237 mixture synthesized by reduction of the corresponding acids, which were isolated and
238 characterized by NMR spectroscopy previously (Lutnaes et al., 2007; Fig. S3, preparation
239 described in SI). C₃₉ isoprenoids were assigned based on chromatographic behavior,
240 molecular formulae generated from accurate mass measurements and characteristic
241 fragment ions (MS² fragmentation patterns are shown in Fig. S1a). For example, the two
242 isomers of GDGTol-0 (highlighted with green circles in Fig. 3e) eluted earlier than those
243 of C_{40/39}-GDGTA-0 (two pink solid line circles in Fig. 3e). In addition, GDGTol-0 and
244 C_{40/39}-GDGTA-0 also have measurably different molecular masses, [M+H]⁺ of m/z:
245 1320.3312 and 1320.2930, respectively and these afford calculated formulae of
246 C₈₆H₁₇₅O₇⁺ for GDGTol-0 and C₈₅H₁₇₁O₈⁺ for C_{40/39}-GDGTA-0. To add weight to this
247 assignment, the fragment ion of m/z: 651.6245 in the MS² of C_{40/39}-GDGTA-0 compared
248 to m/z: 665.6391 of GDGTA-0 represents the loss of methylene from the biphytane (Fig.
249 S1a).

250

251 **3.2. Terminally hydroxylated biphytanyl derivatives**

252

253 Hydrolysis of the glycerol ether bonds in isoprenoidal GDGT generates five types of
254 biphytane-based alcohols, with and without the glycerol backbones, namely, GDGTol,

255 GMGD, GDD, GMM and bpdial (compound structures are given in Fig. S2). For
256 example, we demonstrate their structural relationships to acyclic caldarchaeol, GDGT-0,
257 with a parallel glycerol configuration, a distribution observed in a seep carbonate sample
258 from Marmorito (Fig. 1a and b). Constitutional isomers, which are labeled as peak ‘a’
259 and ‘b’ in the chromatogram of GDGTol, GMGD and GMM in Fig. 1, represent different
260 combinations of *sn*-2 or *sn*-3 glycerol ether bonding. Degradation products of the ring-
261 containing GDGTs are more numerous, due to different possible arrangements of a ring
262 on the biphytanyl chains. A detailed isomeric study of GDGTol, GMGD and GMM and
263 their implications will be discussed in our following works. As for H-GMGTs, which
264 have two biphytane chains linked by a bis-methylene C-C bond at position C₂₀ (Lutnaes
265 et al., 2006; 2007) the cleavage of two glycerol units results in a C₈₀ H-tetrol, instead of
266 two biphytanic diols (bpdials). These hydroxyl derivatives of GDGT were either all, or at
267 least some, present in our sample set comprising extracts of marine sediment, seep
268 carbonate, hydrothermal vent, hot spring sediment and archaeal cell extract (Table 1).

269

270 **3.3. Terminally-carboxylated biphytanyl derivatives**

271

272 Carboxylic acids, corresponding to each of hydroxyl derivatives mentioned above, could
273 logically be generated by oxidation of each terminal alcohol of the biphytane. These were
274 also detected in the analyzed samples and are subsequently referred to as GDGTA for the
275 carboxyl analogue of GDGTol and GMMA for GMM (Fig. 1a, b and Table 1). For
276 isoprenoids possessing two primary hydroxyl groups, such as GDD and bpdial, both
277 mono- and dicarboxyl analogues were detected, with the monocarboxyl derivative of

278 GDD termed GDDA, the dicarboxyl derivative GDDAA, as well as biphytane mono- and
279 diacids. In the case of GMGD, which does not possess a primary biphytane-bound
280 hydroxyl group, no acid derivatives were detected. In the case of H-tetrol, which contains
281 four primary hydroxyl groups on its two linked bpdriols, we detected mono-, di-, tri- and
282 tetraacids in an oily sediment sample collected from a hydrothermal vent site in Guaymas
283 Basin (Fig. 2).

284

285 Under APCI conditions, the ionization patterns of biphytanic monoacid/monool
286 (bpmonoacid/ol) and biphytanic diacids (bpdriacid) differed from bpdriols. A protonated
287 molecular ion $[M+H]^+$ was usually the major ion in mass spectra of bpdriols, while the
288 acids produced more complex mass spectra in our analyses. Dehydrated molecular ions
289 and unknown adducts were formed during the ionization of carboxyl derivatives (Fig. 1b
290 and S1d). The main adduct ions detected were $[M+H+42]^+$ for bpmonoacid/ol and
291 $[M+H+84]^+$ for bpdriacids (Fig. S1d).

292

293 **3.4. C₃₉ and C₃₈ isoprenoids**

294

295 In addition to the series of hydroxylated and carboxylated C₄₀ biphytane derivatives, we
296 identified some with shortened alkyl chains such as the C₃₉ analogues. For example, in
297 most analyzed samples analogues with one methylene unit less than GDGTol and
298 GDGTA, here termed C_{40/39}-GDGTol and C_{40/39}-GDGTA (Arabic numbers represent the
299 carbon number of the two isoprenoidal chains in the molecule), always co-occurred at
300 lower abundance with their C_{40/40} analogues (Fig. 3b, e). C₃₉ derivatives were also

301 detected as analogues of GDD, bpdial and GMM (Fig. 3a, c and d). Additionally, we
302 detected signals that we attribute to the pseudo-homologue of C₃₈ isoprenoids, as
303 GDGTol and GDD (Fig. 3a and b). Within the group of GDDs reduced by two C-atoms,
304 we observed both C_{39/39} and C_{40/38} derivatives (Fig. 3a). Three isomers of the acyclic and
305 four isomers of crenarchaeol-related GDD were detected (Fig. 3a). In previous studies
306 ¹³C depleted C₃₉ head-to-head linked isoprenoids were detected in Cretaceous (Sandy et
307 al., 2012) and Carboniferous seep carbonates (Birgel et al., 2008b); those compounds
308 presumably represent the hydrocarbon derivatives of the C₃₉ functionalized compounds
309 found in this study. Interestingly, no derivatives of C₈₀ H-tetrol and tetraacid with
310 reduced carbon chains were detected in our samples.

311

312 **4. DISCUSSION**

313

314 **4.1. The occurrence of GDGT degradation derivatives in environmental samples**

315

316 The distributions of major degradation derivatives of GDGT-0 and H-GMGT-0 were
317 compared in four representative environmental samples (Fig. 4), which include modern to
318 late Miocene marine subsurface sediment (Leg201-1227), modern hot spring (T-15) and
319 hydrothermally heated sediment (Guaymas Basin 4568), and the Miocene Marmorito
320 seep carbonate. Distinct patterns of degradation derivatives in these four types of samples
321 from different environments and of different age (modern sediments and ancient
322 carbonate rock) reflect variable degrees of degradation and preservation.

323

324 ***4.1.1. Distributions of regular GDGT degradation products in environmental samples***

325

326 The distributions of GDGT degradation products across our sample set suggest that the
327 biological sources of GDGTs, as well as the debris depositional histories, influence the
328 diagenetic trajectory of GDGTs. By way of example, the degradation derivatives of
329 GDGT-0 are around twice as abundant as their precursor in the marine sediment sample
330 of Leg 201-1227, in which bpdial-0 comprises over half of all of the detected degradation
331 products (Fig. 4). However, the GDGT degradation derivatives in Miocene seep
332 carbonates exhibited a lower overall relative abundance, but with a greater variety and
333 portion of relatively labile components, such as the carboxyl derivatives (Table 1 and Fig.
334 4). Regular isoprenoidal GDGTs (as compared to H-GMGTs) preserved in marine
335 sediments are primarily derived from planktonic archaea, dwelling in the water column.
336 In contrast, those in seep carbonates receive a larger *in-situ* contribution from benthic
337 communities engaged in anaerobic oxidation of methane (AOM), as confirmed by low
338 $\delta^{13}\text{C}$ values of biphytanic diacids (cf. Birgel et al., 2008a). The higher proportion of
339 degradation derivatives relative to their GDGT precursors in deep subsurface sediment
340 apparently results from long-term degradation under mild to moderate degradation
341 conditions, with prolonged degradation compared to the Marmorito seep site. Such a
342 long-term diagenetic process is consistent with the influence of the coexisting deep
343 biosphere, which can prevail over many millions of years (e.g. Inagaki et al., 2015). The
344 extraordinarily good preservation of labile compounds in seep carbonates can be
345 attributed to significant *in-situ* GDGT production combined with co-eval carbonate
346 formation and resulting early lithification within methane seepage systems (e.g.,

347 Peckmann et al., 1999; Birgel et al., 2008a), rather than representing input from various
348 sedimentary or sedimentary/planktonic archaea (cf. Feng et al., 2014; Birgel et al., 2008a).

349

350 The relative abundance of degradation products in Guaymas basin sediment is over 40%
351 of all GDGT-derived compounds (Fig. 4). Both biodegradation and thermal diagenesis
352 can be potential sources of degradation products, due to the presence of both active
353 microbial communities and high temperature hydrothermal fluids in Guaymas basin
354 sediments (Teske et al., 2014; Gutierrez et al., 2015). In contrast, there are only low
355 abundances of GDD and bpdial (< 10%) detected as GDGT degradation products in the
356 hot spring sediment (Fig. 4).

357

358 In addition to the contrasting patterns of the different environments, there is a
359 compositional discrepancy between each class of GDGT product within the same sample.
360 For example, previous studies that documented the presence of bpdials and bpdiaacids in
361 environmental samples have shown that the ring distributions and carbon isotopic
362 compositions differ for biphytanes released from coexisting GDGTs (Schouten et al.,
363 1998; Birgel et al., 2008a; Saito and Suzuki, 2010). The Marmorito limestone samples
364 (Fig. 5; Birgel et al. (2008a) provide results on hydrocarbons and bpdiaacids), show
365 distinct ring distribution patterns for GDGT, bpdial, bpdiaacid/ol and bpdiaacid;
366 GDGTs are dominated by GDGT-0 and crenarchaeol, while the relative abundance of
367 tricyclic biphytane derivatives derived from crenarchaeol gradually decreases for the
368 hydroxyl to carboxyl products. Multiple inputs, combined with selective preservation
369 could cause such distributional differences. The ring distribution of GDGTs preserved in

370 sediments may reflect a mixed contribution from both planktonic and benthic species and
371 is frequently dominated by compounds from planktonic sources (Wuchter et al., 2005;
372 Huguet et al., 2007; Lengger et al., 2012). Planktonic and sedimentary archaeal
373 communities could contribute different lipids. Further, compared to biphytanyl products
374 derived from benthic species within the sediment, those derived from the water column
375 will have experienced a very different transportation history. This might explain why the
376 tricyclic diacid derived from planktonic archaea are rare, while the acyclic, mono- and
377 bicyclic diacids with origins from sedimentary methanotrophic archaea, are more
378 common and more ¹³C-depleted in the seep carbonate (isotopic data published in Birgel
379 et al., 2008a).

380

381 *4.1.2. The degradation of H-GMGTs to H-tetrols and H-tetraacids*

382

383 H-GMGT-0 and its hydroxylated degradation products are generally present in the
384 samples from low-temperature and hydrothermal environments (Table 1 and Fig. 4),
385 while compounds with multiple cycloalkyl groups and additional methylations are
386 restricted to the hydrothermal samples alone. In low-temperature samples, H-GMGT-0 is
387 far more abundant than H-GMD-0 (acyclic H-shaped glycerol monoalkyl diether) and
388 tetrol-0 (Fig. 4). The apparently different patterns of H-GMGT-0 and its derivatives,
389 compared to GDGT-0 and its highly abundant degradation products, point to
390 contributions of distinct species and/or different diagenetic pathways.

391

392 We detected H-tetrol and H-tetraacids, and their partially oxidized ‘H-shaped’ mono-, di-
393 and triacid intermediates, in the oily Guaymas Basin sediment (Fig. 2). The occurrence of
394 partially oxidized intermediates, such as the mono-, di- and triacids is more likely a
395 selective and stepwise reaction with enzymatic catalysis rather than chemical diagenesis.
396 H-tetraacids accumulated in naphthenate deposits in oil well infrastructure and pipelines
397 and in crude oils, have distributions usually dominated by 4-8 cyclopentyl rings and 1 or
398 2 additional methyl substitutions (Lutnaes et al., 2007; Sutton & Rowland, 2014).
399 Although H-GMGT-0 is known to be present in a broad range of mesophilic
400 environments (Schouten et al., 2008a), those with multiple cyclizations and methylations
401 have been only detected in hyperthermophilic archaeal species (Schouten et al., 2008b;
402 Knappy et al., 2011; Liu et al., 2012b). H-GMGTs with multiple cyclizations and
403 methylations were detected in both hot spring and Guaymas Basin sediments analyzed.
404 However, H-tetraacids were only found in the oil-impregnated Guaymas Basin sediment
405 (Table 1). In addition to the diagenetic contribution, Lutnaes et al. (2006) also speculated
406 that these tetraacids might be produced by thermophilic, oil-degrading archaea as
407 biosurfactants to facilitate their metabolism. Additional studies would be required to test
408 this hypothesis rigorously. Given the occurrence of biphytane, C₃₉ and smaller head-to-
409 head linked isoprenoids in the geological record, C₃₀ based H-shaped isoprenoidal
410 hydrocarbons might also exist. Whilst these are not detectable with conventional GC-MS,
411 they would be amenable to high temperature GC-MS (cf. Sutton & Rowland, 2012)

412

413 **4.2. The occurrence of GDGT degradation derivatives in archaeal cell extracts**

414

415 In a previous study concerning the characterization of GDD, Liu et al. (2012a) observed
416 the existence of core GDD in the cell extracts of the methanogen *Methanothermococcus*
417 *thermolithotrophicus*. More recently, Meador et al. (2014) reported detection of both
418 core and monoglycosidic GDD (1G-GDD) in a culture of the planktonic ammonia
419 oxidizer *N. maritimus*. Here we extend these observations and report newly identified
420 biphytane derivatives in fresh biomass collected at different growth phases of cell
421 extracts of the archaeon *N. maritimus*. Core lipids accounted for 8.2-15% of the total
422 detected lipids during different growth phases (Elling et al., 2014). We selected the most
423 abundant component, crenarchaeol, to illustrate the distribution of its hydroxyl and
424 carboxyl derivatives in different growth phases. GDD-Cren. and bpdial-Cren. were the
425 only detected hydroxyl components during early exponential growth (Fig. 6); they jointly
426 accounted for less than 1% of all crenarchaeol-based derivatives. In the late growth phase,
427 however, the relative abundances of GDD-Cren. and bpdial-Cren. were almost doubled,
428 while the acid (GDDA-Cren.) and a C₃₉ component (C_{40/39}-GDD-Cren.) emerged as well.
429 GDD-Cren., depleted by two methylene units (C_{39/39} and C_{40/38}-GDD-Cren.), together
430 with GDGTol-Cren. were only observed in the stationary phase.

431

432 Although these derivatives occurred in cell extracts, they cannot be simply attributed as
433 intermediates of GDGT biosynthesis. For example, the carboxyl and C₃₉ based
434 derivatives, such as GDDA and C_{40/39}-GDD, are more likely further oxidized products of
435 GDD. For example, archaeal biphytanyl moieties, synthesized via the mevalonic acid
436 (MVA) or methylerythritol phosphate (MEP) pathways, should have a carbon number
437 that is a multiple of five. Accordingly, the most plausible formation pathway for the C₃₈

438 and C₃₉ moieties is oxidation and decarboxylation of C₄₀ precursors. Formation of C₃₈
439 and C₃₉ moieties via degradation of C₄₀ biphytanyl moieties is also consistent with the
440 higher relative abundance of GDDA and C_{40/39}-GDD during the late stationary phase (Fig.
441 6). The loss of one methylene unit represents an α -oxidation step. A similar well-known
442 enzymatic α -oxidation of isoprenoids is that of phytanic acid (C₂₀) to pristanic acid (C₁₉)
443 by a wide range of organisms (e.g., Rontani and Volkman, 2003; Jansen and Wanders,
444 2006, and other studies cited therein). As in phytanic acid, the C₃ methyl group in
445 biphytanic acid (C₄₀) derivatives prevents an initial β -oxidation mechanism; instead,
446 these compounds undergo α -oxidation to yield C₃₉ based carboxyl isoprenoids. In such a
447 scenario the production of GDD and GDGTol consisting of C₃₈ derivatives would require
448 two successive α -oxidation steps. This is inconsistent with the reported α -oxidation of
449 phytanic acid, which is followed by hydroxylation and then β -oxidation (e.g. Jansen and
450 Wanders, 2006, and other studies cited therein). Therefore, elucidation of the degradation
451 process leading to a C₃₈ isoprenoid requires further study. Furthermore, α - as well as β -
452 oxidation would only result in carboxyl derivatives, and could not explain the occurrence
453 of hydroxyl analogues, such as C_{40/39}-GDD and C_{40/39}-GDGTol (Fig. 3). Although the
454 detection of carboxyl derivatives and C₃₈ and C₃₉ based isoprenoids in a metabolic active
455 culture of *N. maritimus* may imply an intracellular modification of existing C₄₀ based
456 lipids, probably as a result of cell senescence, their contribution is less than 2% of the
457 core lipid fraction, or approximately 0.01% of the entire lipidome. The exact mechanisms
458 responsible for the remarkable proportions (up to 70% in the marine subsurface sediment,
459 Leg201-1227, Fig. 4) of degradation products in environmental samples remain
460 unresolved. The presence of degradation products in archaeal cell extracts, as well as

461 their increase towards later growth and stationary phases, suggests that some are formed
462 rapidly and probably via enzymatic catalysis. On the other hand, the high proportion and
463 diversity of degradation products in the hydrothermally influenced settings also leaves
464 room for an additional role of abiotically-mediated chemical degradation reactions, at
465 least for some of the speculated steps leading via catagenesis from GDGTs to biphytanyl
466 hydrocarbons (cf. Rowland, 1990).

467

468 **4.3. Evidence of analogous behavior of non-isoprenoidal GDGTs**

469 Non-isoprenoidal GDGTs, such as the hypothetical hybrid isoprenoidal/branched GDGT
470 (IB-GDGT) and branched GDGTs, are known to be widely distributed in various
471 environments, although their exact structures and biological source(s) remain unknown
472 (Liu et al., 2012b). The degradation pathways described here are not limited to archaeal
473 GDGTs. For example, in one of the seep carbonate samples, which contains high
474 abundances of branched and IB-GDGTs, non-isoprenoidal GDDs, GMMs and diols have
475 been detected. These possibly represent degradation products of the corresponding
476 branched and IB-GDGTs in the same deposit (Fig. S4 and S5). Our analytical methods
477 also reveal the presence of carboxyl derivatives of these lipids. Non-isoprenoidal
478 GDGTol, GDGTA, GMGD, and their corresponding products with reduced carbon
479 chains (loss of one or two methylene units) were not identified, however, and we attribute
480 this to their low overall abundance in the analyzed samples.

481

482 **5. CONCLUSIONS**

483

484 As with other lipid classes, the intact archaeal tetraethers released from the cells of
485 defunct archaea into various depositional settings, are subjected to diagenesis in
486 sediments. We detected three major classes of GDGT degradation products comprising
487 biphytanyl molecules with terminal hydroxyl, terminal carboxyl and shortened carbon
488 chains. A hypothetical scheme of the GDGT degradation pathway to rationalize such a
489 pathway is illustrated in Fig. 7. The labile polar head groups of intact GDGTs, as they
490 occur in living cells, are initially lost to produce the more recalcitrant core GDGTs.
491 Hydrolysis of the different ether bonds then, as we suggest, results in discrete series of
492 hydroxyl derivatives composed of one or two glycerol and biphytanol units. Oxidation of
493 each terminal hydroxyl functional group may then generate related carboxyl products.
494 Elimination of the C₁ carbon via α -oxidation and subsequent β -oxidation steps, will likely
495 convert the C₄₀ biphytanyl based compounds into shortened isoprenoids, such as C_{40/39}-
496 GDGTA and C_{40/39}-GDGTol. Further chemical or biological alteration of these
497 intermediates may over geological time, result in the C₄₀, C₃₉ and smaller head-to-head
498 linked isoprenoidal hydrocarbons reported to occur in petroleum and marine deposits.
499
500 A multitude of diagenetic processes will lead to the degradation of GDGTs in sediments.
501 However, we also observed the accumulation of C₃₉ based carboxyl isoprenoids in the
502 later growth and stationary phases of an archaeal cell culture. This implies that enzymatic
503 pathways for degradation of GDGTs also exist, very likely, as a response to substrate
504 limitation, senescence or cell lysis. Additional studies will be required to study this facet
505 in greater detail.
506

507 The detection of H-GMGT, H-GMD, H-tetrols and their further oxidized carboxyl
508 intermediates in the oil-contaminated sediments of Guaymas Basin elucidated a
509 formation pathway from H-GMGT to H-tetraacids under anoxic conditions.
510 Metagenomic data for samples from the Guaymas Basin and especially sediment with oil
511 impregnation may help to elucidate the origin of H-tetraacids further.
512
513 In various geological settings these hydroxyl and carboxyl derivatives co-occur with their
514 GDGT precursors, including both isoprenoidal and non-isoprenoidal GDGTs. Our
515 analysis of their distributions in environmental samples and archaeal cell extracts
516 represents an initial effort to document the possible diagenetic pathways of GDGTs and
517 to bring about the same level of understanding that we have for steroids and triterpenoids.
518

519

520 **ACKNOWLEDGEMENTS**

521

522 X.-L.L. was funded by European Union's Seventh Framework Programme–“Ideas”
523 Specific Programme, ERC grant agreement No. 247153 (Advanced Grant DARCLIFE;
524 PI K.-U.H.), the Simons Foundation Collaboration on the Origins of Life (SCOL).
525 Cultivation experiments and lipid analyses at the University of Bremen were funded by
526 the Deutsche Forschungsgemeinschaft through the Gottfried Wilhelm Leibniz Prize
527 awarded to K.-U.H. (Hi 616-14-1). SJR and PAS were funded by a European Research
528 Council Advanced Investigators Award to SJR for project OUTREACH (agreement no.
529 228149). We thank Dr. Ann Pearson, Dr. Yoshinori Takano and two anonymous
530 reviewers for their constructive comments on this work.

531

532 **REFERENCES**

533

- 534 Baugh T.D., Wolf N.O., Mediaas H., Vindstad J.E. and Grande K. (2004)
535 Characterization of a Calcium Naphthanate Deposit -The ARN Acid Discovery.
536 Preprints/American Chemical Society, Division of Petroleum Chemistry **49**, 274–276.
- 537 Baugh T.D., Grande K.V., Mediaas H., Vindstad J.E. and Wolf N.O. (2005) In The
538 Discovery of High Molecular Weight Naphthenic Acids (ARN Acid) Responsible for
539 Calcium Naphthenate Deposits. SPE International Symposium on Oilfield Scale,
540 Aberdeen, U.K., May 11–12 2005; SPE 93011.
- 541 Becker K.W., Lipp J.S., Zhu C., Liu X.-L. and Hinrichs K.-U. (2013) An improved
542 method for the analysis of archaeal and bacterial ether core lipids. *Org. Geochem.* **61**,
543 34-44.
- 544 Birgel, D., Thiel, V., Hinrichs, K.-U., Elvert, M., Campbell, K.A., Reitner, J., Farmer,
545 J.D. and Peckmann, J. (2006) Lipid biomarker patterns of methane-seep microbialites
546 from the Mesozoic convergent margin of California. *Org. Geochem.* **37**, 1289–1302.
- 547 Birgel, D. and Peckmann, J. (2008) Aerobic methanotrophy at ancient marine methane
548 seeps: a synthesis. *Org. Geochem.* **39**, 1659–1667.
- 549 Birgel D., Elvert M., Han X. and Peckmann J. (2008a) ¹³C-depleted biphytanic diacids as
550 tracers of past anaerobic oxidation of methane. *Org. Geochem.* **39**, 152–156.
- 551 Birgel, D., Himmler, T., Freiwald, A. and Peckmann, J. (2008b) A new constraint on the
552 antiquity of anaerobic oxidation of methane: Late Pennsylvanian seep limestones
553 from southern Namibia. *Geology* **36**, 543–546.
- 554 Brocks J.J. and Schaeffer P. (2008) Okenane, a biomarker for purple sulfur bacteria
555 (Chromatiaceae), and other new carotenoid derivatives from the 1640 Ma Barney
556 Creek Formation. *Geochim. Cosmochim. Acta* **72**, 1396–1414.
- 557 Chappe B., Albrecht P. and Michaelis W. (1982) Polar lipids of archaebacteria in
558 sediments and petroleums. *Science* **217**, 65–66.
- 559 Clari P., Gagliardi C., Governa M.E., Ricci B. and Zuppi G.M. (1988) I calcari de
560 Marmorito: Una testimonianza di processidiagene- tici in presenza di metano. *Boll*
561 *Museo Regionale Sci Naurali Torino* **6**, 197–216.
- 562 Clari P., Fornara L., Ricci B. and Zuppi G.M. (1994) Methane-derived carbonates and
563 chemosymbiotic communities of Piedmont (Miocene, northern Italy): an update.
564 *Geo-Marine Lett.* **14**, 201–209.
- 565 Elling F.J., Könneke M., Lipp J.S., Becker K.W., Gagen E.J. and Hinrichs K.-U. (2014)
566 Effects of growth phase on the membrane lipid composition of the thaumarchaeon
567 *Nitrosopumilus maritimus* and their implications for archaeal lipid distributions in the
568 marine environment. *Geochim. Cosmochim. Acta* **141**, 579–597.

- 569 Feng D., Birgel D., Peckmann J., Roberts H. H., Joye S. B., Sassen R., Liu X.-L.,
570 Hinrichs K.-U. and Chen D. (2014) Time integrated variation of sources of fluids and
571 seepage dynamics archived in authigenic carbonates from Gulf of Mexico Gas
572 Hydrate Seafloor Observatory. *Chem. Geol.* **385**, 129–139.
- 573 Gutierrez, T., Biddle, J.F., Teske, A. and Aitken, M.D. (2015) Cultivation-dependent and
574 cultivation-independent characterization of hydrocarbon-degrading bacteria in
575 Guaymas Basin sediments. *Front. Microbiol.* **6**, doi: 10.3389/fmicb.2015.00695
- 576 Harvey, H.R., Fallon, R.D. and Patton, J.S. (1986) The effect of organic matter and
577 oxygen on the degradation of bacterial membrane lipids in marine sediments.
578 *Geochim. Cosmochim. Acta* **50**, 795–804.
- 579 Huguet, C., Schimmelmann, A., Thunell, R., Lourens, L.J., Sinninghe Damsté, J.S. and
580 Schouten, S. (2007) A study of the TEX₈₆ paleothermometer in the water column and
581 sediments of the Santa Barbara Basin, California. *Paleoceanography* **22**,
582 doi:10.1029/2006PA001310
- 583 Inagaki, F., et al. (2015), Exploring deep microbial life in coal-bearing sediment down to
584 2.5 km below the ocean floor, *Science*, **349**, 420–424,
- 585 Innes, H.E., Bishop, A.N., Head, I.M. and Farrimond, P. (1997) Preservation and
586 diagenesis of hopanoids in Recent lacustrine sediments of Priest Pot, England. *Org.*
587 *Geochem.* **26**, 565-576.
- 588 Jansen G.A. and Wanders R.J.A. (2006) Alpha-Oxidation. *Biochim Biophys Acta – Mol.*
589 *Cell* **1763**, 1403–1412.
- 590 Könneke M., Bernhard A. E., de la Torre J. R., Walker C. B., Waterbury J. B. and Stahl
591 D. A. (2005) Isolation of an autotrophic ammonia-oxidizing marine archaeon.
592 *Nature* **437**, 543–546.
- 593 Knappy, C.S., Nunn, C.E.M., Morgan, H.W. and Keely, B.J. (2011) The major lipid cores
594 of the archaeon *Ignisphaera aggregans*: implications for the phylogeny and
595 biosynthesis of glycerol monoalkyl glycerol tetraether isoprenoid lipids.
596 *Extremophiles* **15**, 517–528.
- 597 Knappy C.S. and Keely B.J. (2012) Novel glycerol dialkanol triols in sediments:
598 transformation products of glycerol dibiphytanyl glycerol tetraether lipids or
599 biosynthetic intermediates? *Chem. Commun.* **48**, 841–843.
- 600 Kuypers, M. M. M., Blokker, P., Erbacher, J., Kinkel, H., Pancost, R. D., Schouten, S. and
601 Sinninghe Damsté, J. S. (2001) Massive expansion of marine Archaea during a
602 mid-Cretaceous oceanic anoxic event. *Science* **293**, 92-95.
- 603 Lengger, S.K., Hopmans, E.C., Reichart, G.-J., Nierop, K.G.J., Damsté, J.S.S. and
604 Schouten, S. (2012) Intact polar and core glycerol dibiphytanyl glycerol tetraether
605 lipids in the Arabian Sea oxygen minimum zone. Part II: Selective preservation and
606 degradation in sediments and consequences for the TEX₈₆. *Geochim. Cosmochim.*

- 607 *Acta* **98**, 244–258.
- 608 Lipp J.S. and Hinrichs K.-U. (2009) Structural diversity and fate of intact polar lipids in
609 marine sediments. *Geochim. Cosmochim. Acta* **73**, 6816–6833.
- 610 Liu, X.-L., Lipp, J.S. and Hinrichs, K.-U. (2011) Distribution of intact and core GDGTs
611 in marine sediments. *Org. Geochem.* **42**, 368–375.
- 612 Liu X.-L., Lipp J.S., Schröder J.M., Summons R.E. and Hinrichs K.-U. (2012a)
613 Isoprenoid glycerol dialkanol diethers: A series of novel archaeal lipids in marine
614 sediments. *Org. Geochem.* **43**, 50–55.
- 615 Liu X.-L., Summons R.E. and Hinrichs K.-U. (2012b) Extending the known range of
616 glycerol ether lipids in the environment: structural assignments based on tandem
617 mass spectral fragmentation patterns. *Rapid Commun. Mass Spectrom.* **26**, 2295–
618 2302.
- 619 Lunau M., Lemke A., Walther K., Martens-Habbena W. and Simon M. (2005) An
620 improved method for counting bacteria from sediments and turbid environments by
621 epifluorescence microscopy. *Environ. Microbiol.* **7**, 961–968.
- 622 Lutnaes B.F., Brandal Ø., Sjöblom J. and Krane J. (2006) Archaeal C₈₀ isoprenoid
623 tetraacids responsible for naphthenate deposition in crude oil processing. *Org.*
624 *Biomol. Chem.* **4**, 616.
- 625 Lutnaes B.F., Krane J., Smith B.E. and Rowland S.J. (2007) Structure elucidation of C₈₀,
626 C₈₁ and C₈₂ isoprenoid tetraacids responsible for naphthenate deposition in crude oil
627 production. *Org. Biomol. Chem.* **5**, 1873.
- 628 Mackenzie, A.S., Brassell, S.C., Eglinton, G. and Maxwell, J.R. (1982) Chemical fossils
629 – the geological fate of steroids. *Science* **217**, 491–504.
- 630 Martens-Habbena W., Berube P.M., Urakawa H., de la Torre J.R. and Stahl D.A. (2009)
631 Ammonia oxidation kinetics determine niche separation of nitrifying Archaea and
632 Bacteria. *Nature* **461**, 976–979.
- 633 Meador T.B., Zhu C., Elling F.J., Könneke M. and Hinrichs K.-U. (2014) Identification
634 of isoprenoid glycosidic glycerol dibiphytanol diethers and indications for their
635 biosynthetic origin. *Org. Geochem.* **69**, 70–75.
- 636 Meador, T.B., Bowles, M., Lazar, C., Zhu, C., Teske, A. and Hinrichs, K.-U. (2015) The
637 archaeal lipidome in estuarine sediment dominated by members of the miscellaneous
638 Crenarchaeotal Group. *Environ. Microbiol.* **17**, 2441–2458.
- 639 Meunier-Christman C. (1988) Géochimie organique de phosphates et schistes bitumineux
640 marocains: étude du processus de phosphatogenèse. PhD thesis, University of
641 Strasbourg, p. 133.
- 642 Moldowan J.M. and Seifert W.K. (1979) Head-to-head linked isoprenoid hydrocarbons in

- 643 petroleum. *Science* **204**, 169–171.
- 644 Morii, H., Eguchi, T., Nishihara, M., Kakinuma, K., König, H. and Koga, Y. (1998) A
645 novel ether core lipid with H-shaped C₈₀-isoprenoid hydrocarbon chain from the
646 hyperthermophilic methanogen *Methanothermus fervidus*. *Biochim. Biophys. Acta*
647 **1390**, 339–345.
- 648 Peckmann, J., Thiel, V., Michaelis, W., Clari, P., Gaillard, C., Martire, L. and Reitner, J.
649 (1999) Cold seep deposits of Beauvoisin (Oxfordian; southeastern France) and
650 Marmorito (Miocene; northern Italy): microbially induced authigenic carbonates. *Int.*
651 *J. Earth Sci.* **88**, 60–75.
- 652 Pearson, A., Seewald, J.S. and Eglinton, T.I. (2005) Bacterial incorporation of relict
653 carbon in the hydrothermal environment of Guaymas Basin. *Geochim. Cosmochim.*
654 *Acta* **69**, 5477–5486.
- 655 Pearson, A. and Ingalls, A.E. (2013) Assessing the use of Archaeal lipids as marine
656 environmental proxies. *Annu. Rev. Earth Planet. Sci.* **41**, 359–384.
- 657 Pease, T.K., Van Vleet, E.S., Barre, J.S. and Dickins, H.D. (1998) Degradation of
658 glyceryl ethers by hydrous and flash pyrolysis. *Org. Geochem.* **29**, 979–988.
- 659 Peters, K. E., Walters, C. C. and Moldowan, J. M. (2004) The biomarker guide, 2nd edn.
660 Cambridge, UK: Cambridge University Press.
- 661 Rontani J.-F. and Volkman J.K. (2003) Phytol degradation products as biogeochemical
662 tracers in aquatic environments. *Org. Geochem.* **34**, 1–35.
- 663 Rowland, S.J. (1990) Production of acyclic isoprenoid hydrocarbons by laboratory
664 maturation of methanogenic bacteria. *Org. Geochem.* **15**, 9–16.
- 665 Sandy, M. R., Lazăr, I., Peckmann, J., Birgel, D., Stoica, M. and Roban, R. D. (2012)
666 Methane-seep brachiopod fauna within turbidites of the Sinaia Formation, Eastern
667 Carpathian Mountains, Romania. *Palaeogeogr. Palaeoclimatol. Palaeoecol.* **323-325**,
668 42-59.
- 669 Saito H. and Suzuki N. (2010) Distribution of acyclic and cyclic biphytandiols in recent
670 marine sediments from IODP Site C0001, Nankai Trough. *Org. Geochem.* **41**, 1001–
671 1004.
- 672 Schouten S., Hoefs M.J., Koopmans M.P., Bosch H.-J. and Sinninghe Damsté J.S. (1998)
673 Structural characterization, occurrence and fate of archaeal ether-bound acyclic and
674 cyclic biphytanes and corresponding diols in sediments. *Org. Geochem.* **29**, 1305–
675 1319.
- 676 Schouten, S., Wakeham, S. G., Hopmans, E. C. and Sinninghe Damsté, J. S. (2003)
677 Biogeochemical evidence that thermophilic archaea mediate the anaerobic oxidation
678 of methane. *Appl. Environ. Microbiol.* **69**, 1680-1686.
- 679 Schouten, S., Baas, M., Hopmans, E.C. and Sinninghe Damsté, J.S. (2008a) An unusual

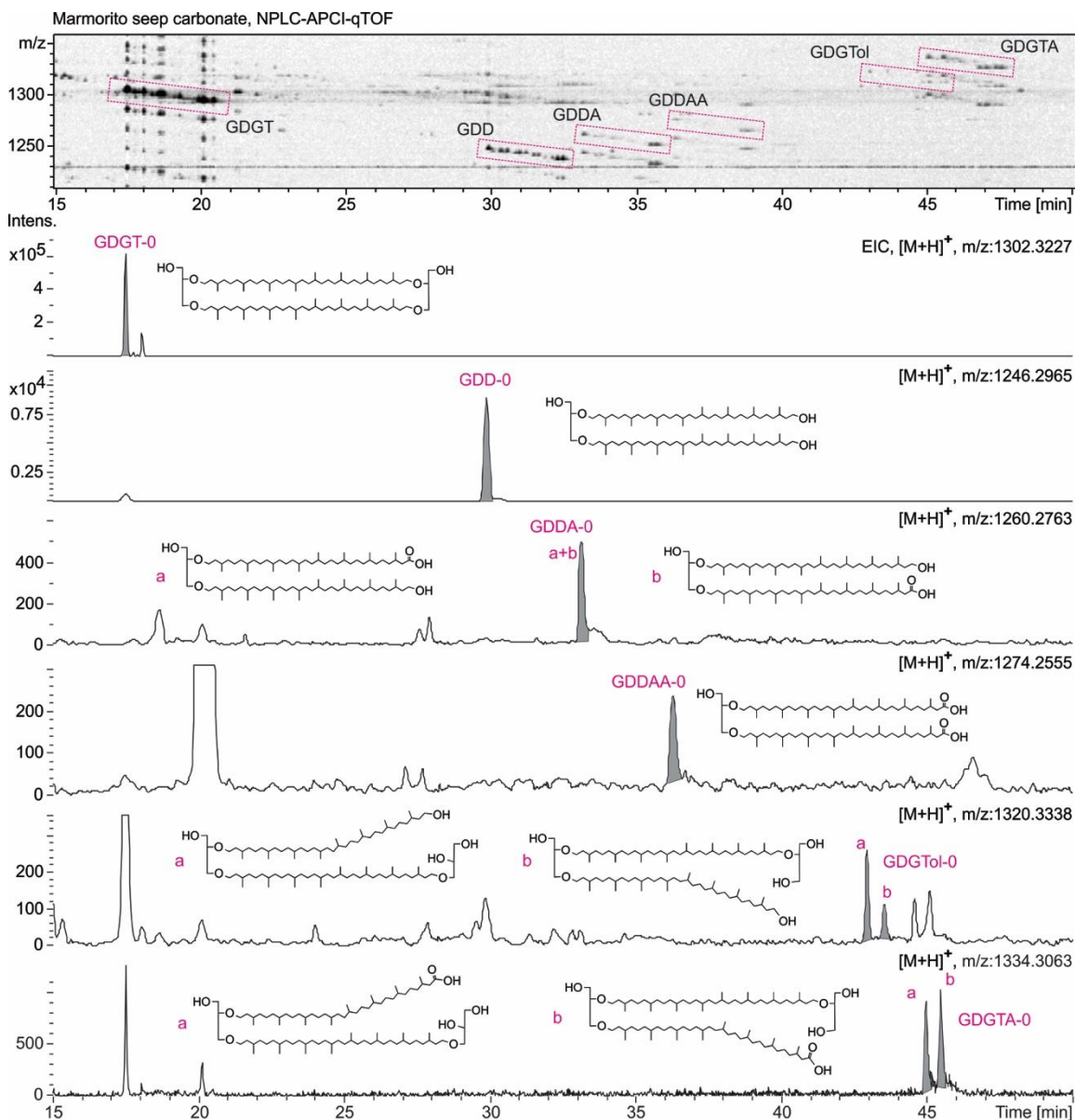
- 680 isoprenoid tetraether lipid in marine and lacustrine sediments. *Org. Geochem.* **39**,
681 1033–1038.
- 682 Schouten, S., Baas, M., Hopmans, E.C., Reysenbach, A.-L. and Sinninghe Damsté, J.S.
683 (2008b) Tetraether membrane lipids of Candidatus “*Aciduliprofundum boonei*”, a
684 cultivated obligate thermoacidophilic euryarchaeote from deep-sea hydrothermal
685 vents. *Extremophiles* **12**, 119–124.
- 686 Schouten, S., Hopmans, E.C. and Sinninghe Damsté, J.S. (2013) The organic
687 geochemistry of glycerol dialkyl glycerol tetraether lipids: A review. *Org. Geochem.*
688 **54**, 19–61.
- 689 Stickland J.D.H. and Parsons T.R.A. (1972) A Practical Handbook of Seawater Analysis.,
690 Fisheries Research Board of Canada, Ottawa.
- 691 Sturt H. F., Summons R. E., Smith K., Elvert M. and Hinrichs K.-U. (2004) Intact polar
692 membrane lipids in prokaryotes and sediments deciphered by high-performance
693 liquid chromatography/electrospray ionization multistage mass spectrometry - new
694 biomarkers for biogeochemistry and microbial ecology. *Rapid Commun. Mass*
695 *Spectrom.* **18**, 617–628.
- 696 Sutton, P.A. and Rowland, S.J. (2012) High temperature gas chromatography–time-of-
697 flight-mass spectrometry (HTGC–ToF-MS) for high-boiling compounds. *J.*
698 *Chromatogr. A.* **1243**, 69–80.
- 699 Sutton, P.A. and Rowland, S.J. (2014) Determination of the content of C₈₀ tetraacids in
700 petroleum. *Energy Fuels* **28**, 5657–5669.
- 701 Teske, A., Callaghan, A.V. and LaRowe, D.E. (2014) Biosphere frontiers of subsurface
702 life in the sedimented hydrothermal system of Guaymas Basin. *Front. Microbiol.* **5**,
703 doi:10.3389/fmicb.2014.00362
- 704 Thiel, V., Peckmann, J., Seifert, R., Wehrung, P., Reitner, J. and Michaelis, W. (1999)
705 Highly isotopically depleted isoprenoids: molecular markers for ancient methane
706 venting. *Geochim. Cosmochim. Acta* **63**, 3959–3966.
- 707 Weijers, J.W.H., Schouten, S., Hopmans, E.C., Geenevasen, J.A.J., David, O.R.P.,
708 Coleman, J.M., Pancost, R.D. and Sinninghe Damsté, J.S. (2006) Membrane lipids
709 of mesophilic anaerobic bacteria thriving in peats have typical archaeal traits.
710 *Environ. Microbiol.* **8**, 648–657.
- 711 Wuchter, C., Schouten, S., Wakeham, S.G. and Sinninghe Damsté, J.S. (2005) Temporal
712 and spatial variation in tetraether membrane lipids of marine Crenarchaeota in
713 particulate organic matter: Implications for TEX₈₆ paleothermometry.
714 *Paleoceanography* **20**, doi:10.1029/2004PA001110
- 715 Xie, S., Lipp, J.S., Wegener, G., Ferdelman, T.G. and Hinrichs, K.-U. (2013) Turnover of

- 716 microbial lipids in the deep biosphere and growth of benthic archaeal populations.
717 *Proc. Natl. Acad. Sci. USA* **110**, 6010-6014.
- 718 Yang H., Pancost R.D., Tang C., Ding W., Dang X. and Xie S. (2014) Distributions of
719 isoprenoid and branched glycerol dialkanol diethers in Chinese surface soils and a
720 loess–paleosol sequence: Implications for the degradation of tetraether lipids. *Org.*
721 *Geochem.* **66**, 70–79.
- 722 Yoshinaga, M.Y., Lazar, C.S., Elvert, M., Lin, Y-S., Zhu, C., Heuer, V.B., Teske, A. and
723 Hinrichs, K.-U. (2015) Possible roles of uncultured archaea in carbon cycling in
724 methane-seep sediments. *Geochim. Cosmochim. Acta*, **164**, 35-52.
- 725 Zhu, R., Evans, T.W., Wörmer, L., Lin, Y.-S., Zhu, C. and Hinrichs, K.-U. (2013a)
726 Improved sensitivity of sedimentary phospholipid analysis resulting from a novel
727 extract cleanup strategy. *Org. Geochem.* **65**, 46–52.
- 728 Zhu C., Lipp J.S., Wörmer L., Becker K.W., Schröder J. and Hinrichs K.-U. (2013b)
729 Comprehensive glycerol ether lipid fingerprints through a novel reversed phase liquid
730 chromatography–mass spectrometry protocol. *Org. Geochem.* **65**, 53–62.

Compounds	Abbreviation	Structural illustration	Distribution				
			Leg201-1227	Marmorito carbonate	Guaymas Basin 4568	Hot Spring-15	N. maritimus stat. phase
glycerol dialkyl glycerol tetraether	GDGT		+	+	+	+	+
glycerol dialkyl glycerol triether alcohol	GDGTol		+	+	+	n.d.	+
glycerol dialkyl glycerol triether acid	GDGTA		+	+	n.d.	n.d.	n.d.
glycerol dibiphytanol diether	GDD		+	+	+	+	+
glycerol dibiphytanol diether monoacid	GDDA		+	+	+	n.d.	+
glycerol dibiphytanol diether diacid	GDDAA		n.d.	+	n.d.	n.d.	n.d.
glycerol monobiphytanyl glycerol diether	GMGD		+	+	+	n.d.	n.d.
glycerol monobiphytanol monoether	GMM		+	+	+	n.d.	n.d.
glycerol monobiphytanol monoether diacid	GMMA		n.d.	+	n.d.	n.d.	n.d.
biphytanic diol	bpdiol		+	+	+	+	+
biphytanic monoacid	bpmonoacid/ol		+	+	n.d.	n.d.	n.d.
biphytanic diacid	bpdiacid		n.d.	+	n.d.	n.d.	n.d.
H-shaped glycerol monoalkyl glycerol tetraether	H-GMGT		+	+	+	+	n.d.
H-shaped glycerol monoalkyl diether	H-GMD		+	+	+	+	n.d.
H-shaped C ₈₀ tetrol	H-tetrol		+	+	+	+	n.d.
H-shaped C ₈₀ monoacid	H-monoacid		n.d.	n.d.	+	n.d.	n.d.
H-shaped C ₈₀ diacid	H-diacid		n.d.	n.d.	+	n.d.	n.d.
H-shaped C ₈₀ triacid	H-triacid		n.d.	n.d.	+	n.d.	n.d.
H-shaped C ₈₀ tetraacid	H-tetraacid		n.d.	n.d.	+	n.d.	n.d.

732 **Table 1.** Compound classes discussed in the paper. Illustrated structures show only the
733 acyclic biphytane derivatives. Constitutional isomers are not included. Representative
734 samples showing the distribution of GDGT and degradation products in various
735 environment settings and cell. '+' compound detected, 'n.d.' compound not detected.

736



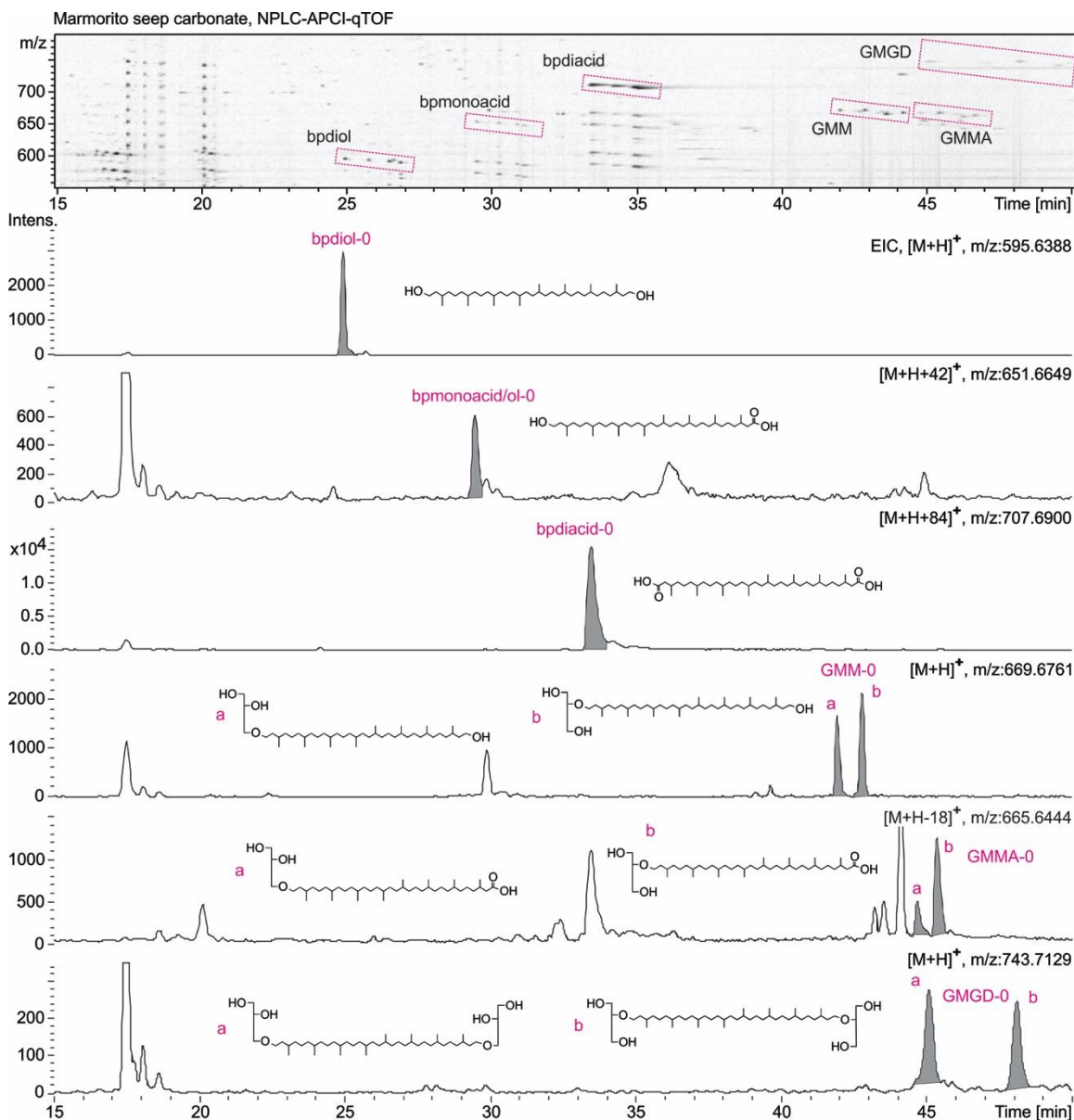
737

738 **Fig. 1a**

739 Density maps and extracted ion chromatograms (EICs) of NPLC-APCI-qTOF showing
 740 the detection of isoprenoidal GDGT-0 and its hydroxylated and carboxylated derivatives
 741 with two (Fig. 1a) or one biphytane units (Fig. 1b) in the Marmorito seep carbonate.

742 Multiple isomers were observed for GDDA, GDGTol, GDGTA, GMM and GMGD and
 743 are labeled as 'a' and 'b'. The isomeric composition of GMGD, 'a' and 'b', may provide
 744 insights regarding the regioisomerism of GDGTs and will be subject of a future report.

745



746

747

748 Fig. 1b

749 Density maps and EICs of NPLC-APCI-qTOF showing the detection of isoprenoidal

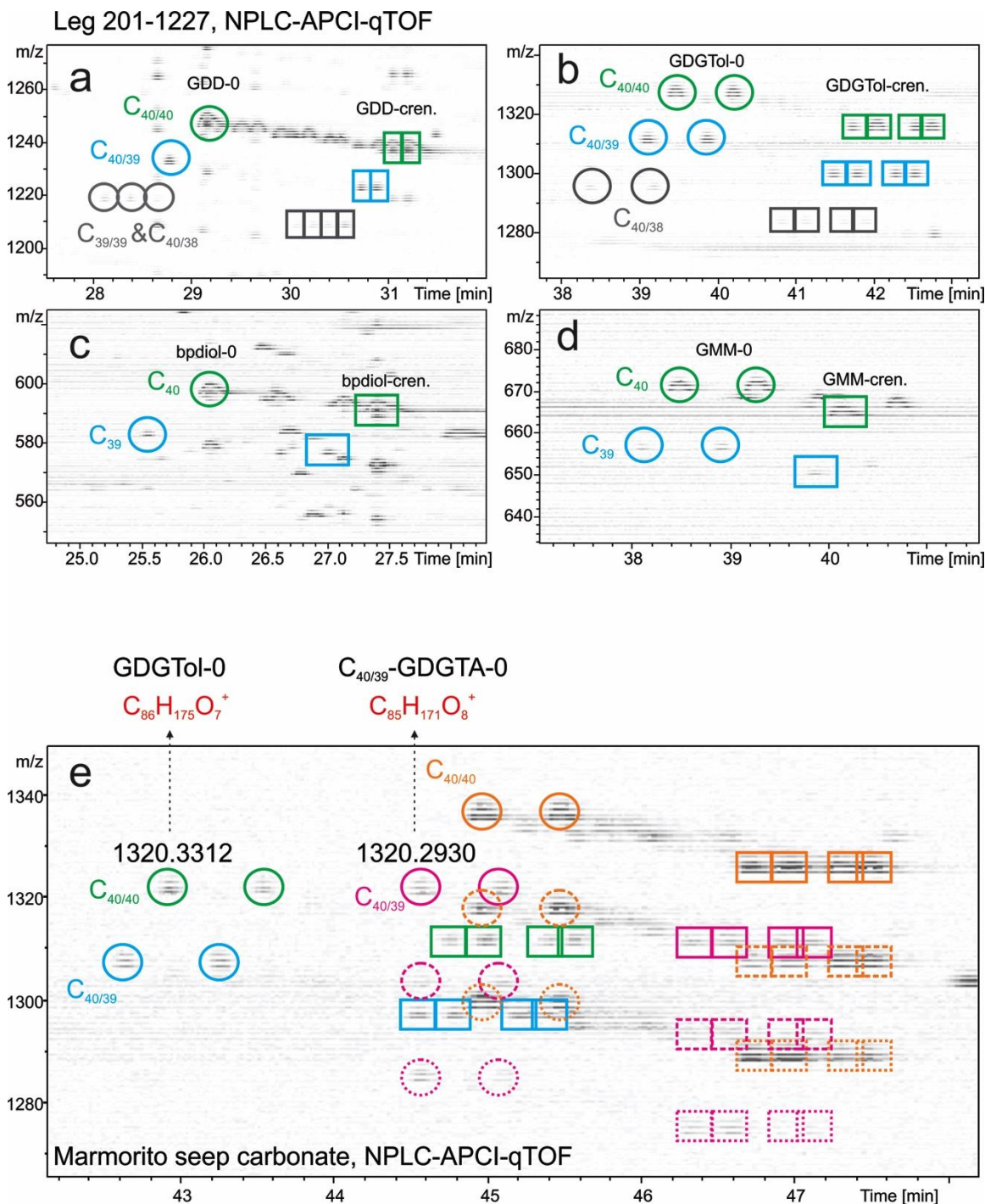
750 GDGT-0 and hydroxylated and carboxylated derivatives with two (Fig. 1a) or one,

751 biphytane units (Fig. 1b) in the Marmorito seep carbonate. Multiple isomers were

752 observed for GDDA, GDGTol, GDGTA, GMM and GMGD and are labeled as 'a' and

753 'b'. The isomeric composition of GMGD, 'a' and 'b', may provide insights regarding the

754 regioisomerism of GDGTs.



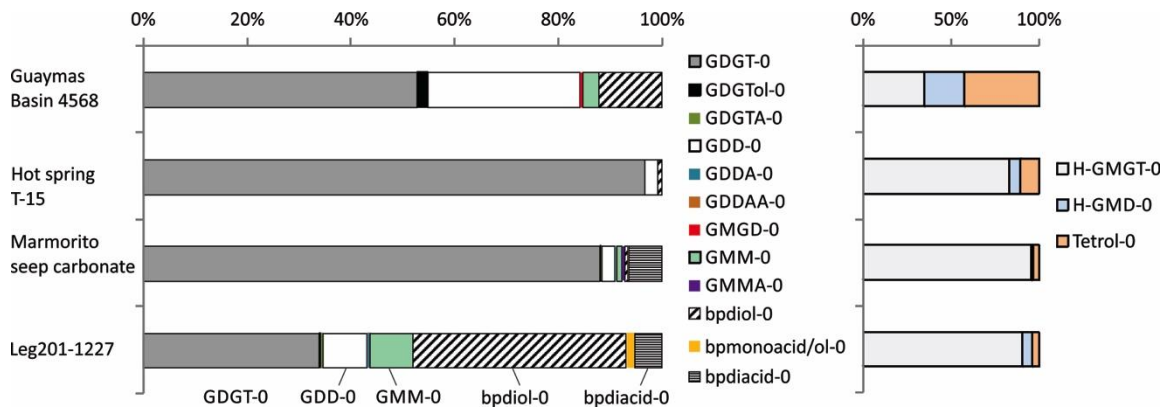
769

770 Fig. 3 Density maps of NPLC-APCI-qTOF showing in one marine sediment (Leg 201-
 771 1227) the detection of GDD, GDGTol, biphytane diol, GMM and their co-occurring
 772 further degradation derivatives with C_{39} and C_{38} based isoprenoids, (a-d). Highlighted are
 773 the most dominant components including the GDGT-0 (open circle) and crenarchaeol-
 774 related (rectangle) compounds. Different compound classes are also color coded. C_{40}

775 hydroxyl derivatives are in green, C₃₉ in blue and the C₃₈ related in grey, C₄₀ carboxyl
776 derivatives are in orange and C₃₉ in pink. Multiple isomers occur due to different ether
777 bonding and ring arrangements. The occurrence of C_{40/39}-GDGTA was shown in one
778 sample of Marmorito seep carbonate (e). The molecular ion of C_{40/39}-GDGTA-0 and
779 GDGTol-0 gives similar but distinguishable masses, m/z: 1320.2930 and 1320.3312,
780 respectively. Under APCI, dehydrated ions of carboxyl derivatives occurred (highlighted
781 ions with dashed lines).

782

783



784

785

786 Fig. 4 Relative abundances of diagenetic derivatives of GDGT-0 (left panel) and H-

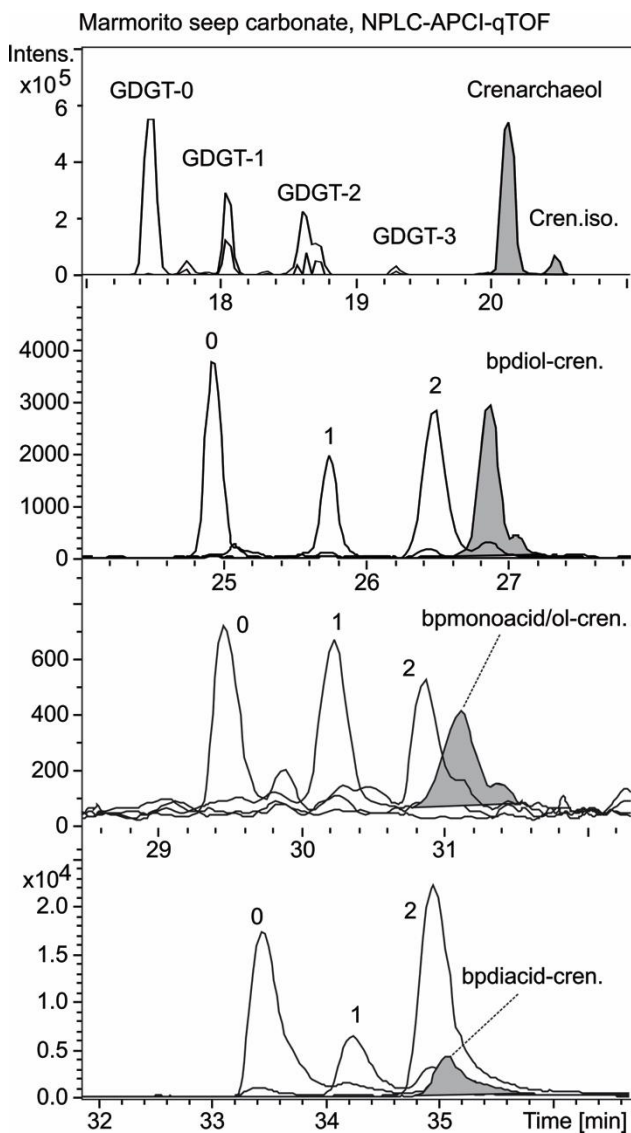
787 GMGT-0 (right panel) in four representative environmental samples.

788

789

790

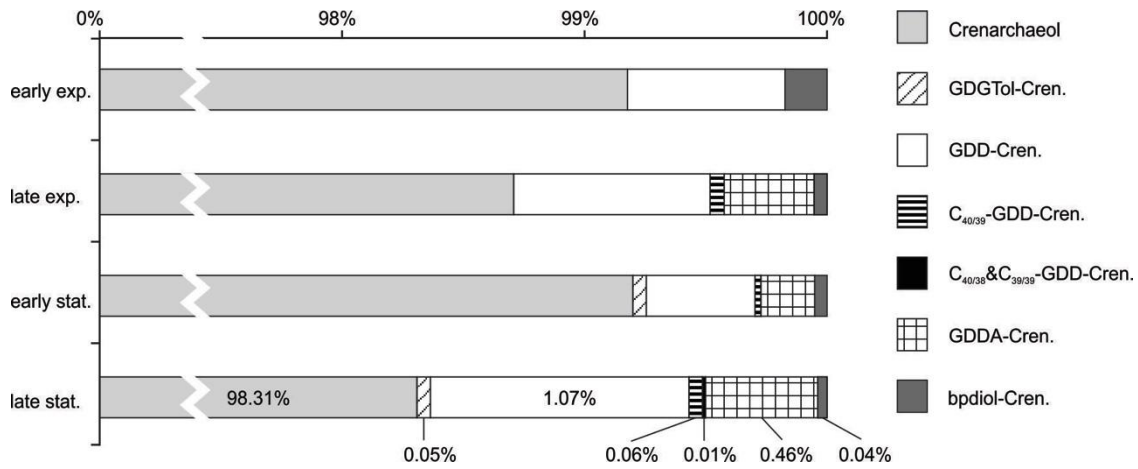
791



792

793 Fig. 5 Extracted ion chromatograms from NPLC-APCI-qTOF analysis, showing the
 794 distribution of GDGT, bpdial, bpmonoacid/ol and bpdiaacids in a seep carbonate,
 795 Marmorito. Peaks of crenarchaeol and its related derivatives are shaded; crenarchaeol
 796 derivatives have decreased abundances in the acid fractions.
 797

798



799

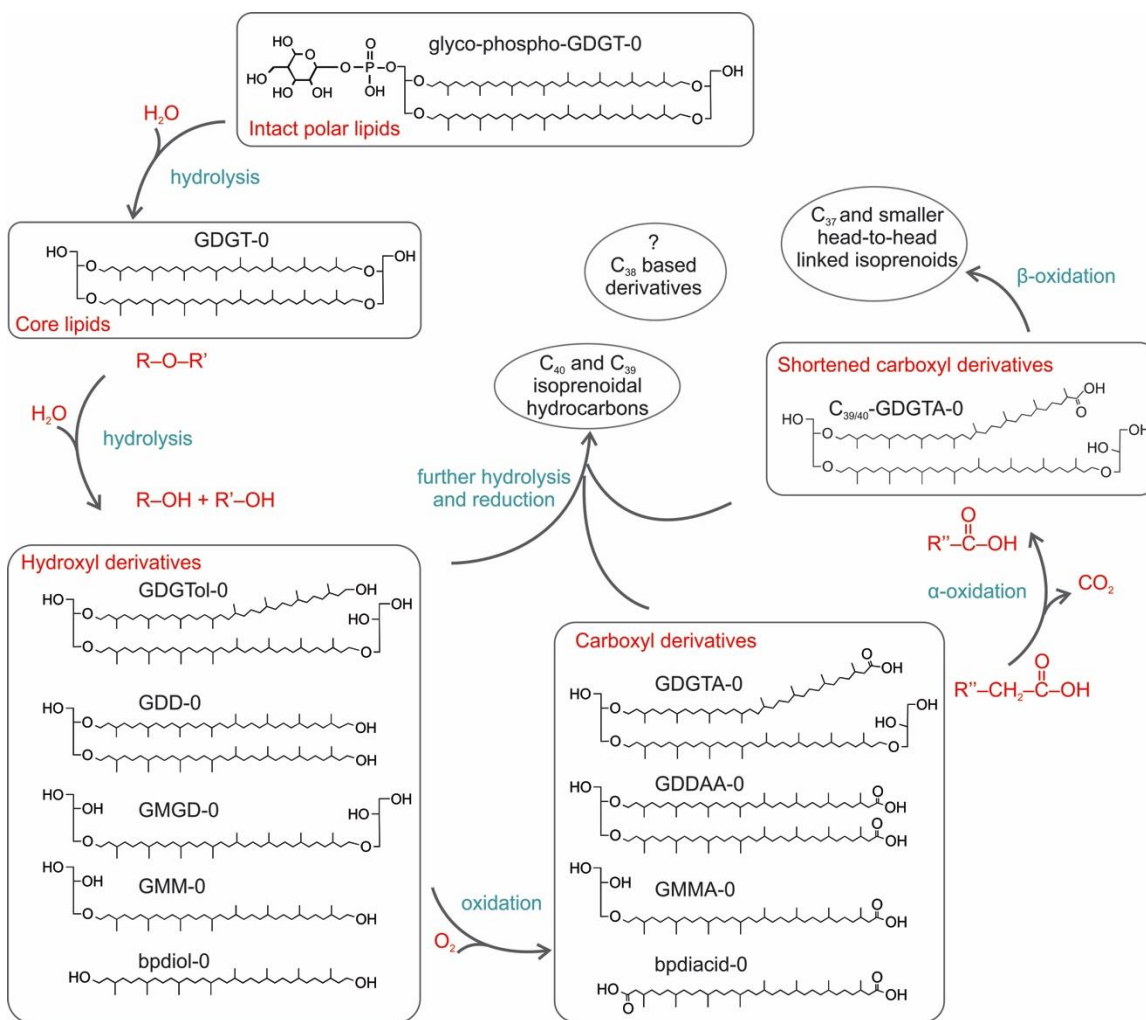
800

801

802 Fig. 6 The relative abundance of core crenarchaeol and its related hydroxyl, carboxyl and

803 C₃₉ and C₃₈ based derivatives in different growth phases of *N. maritimus*.

804



806

807 Fig. 7 Hypothetical scheme showing the suggested diagenetic pathways of GDGTs.

808 GDGT-0 and its related IPL and degradation derivatives are used as an example. In the

809 flow chart, R, R' and R'' represent different alkyl chains. Intermediate components, such

810 as GDDA, bpdmonoacid/ol are not included. The formation of C₃₈ based isoprenoids is not811 clear and thus is labeled with '?'.
812

813

813

814 **Supplementary information**

815

816 **Sample preparation**

817

818 **1. Hot spring sediment T-15**

819 Sediment was collected from the bottom of a geothermal well located in Ruidian (Jinze
820 hot spring: N 25.44138°, E98.46004°, Elevation:1740m. Tengchong County, Yunnan
821 Province, China), with water pH of 6.71 and temperature of 80.6 °C. Roughly 5 g of
822 freeze-dried sediment was extracted in an ultrasonic bath with methanol (MeOH; twice),
823 methanol-dichloromethane (DCM; 1:1, v/v; twice) and finally DCM (twice). All
824 supernatants were collected in a flask and completely dried under N₂. The total lipid
825 extract was fractionated over a pre-activated silica gel chromatography into apolar
826 (alkane) and polar (intact polar GDGTs and GDGT core lipids) fractions using *n*-hexane-
827 DCM (9:1, v/v) and DCM-MeOH (1:1, v/v) as eluents respectively. The polar fraction
828 was used for the lipid analysis in this study.

829

830 **2. H-tetrol standards**

831 An oilfield calcium naphthenate deposit was Soxhlet extracted sequentially
832 (dichloromethane/*n*-hexane, 1/1, v/v, 300 mL, 8h; toluene/acetone, 3/2, v/v, 250 mL, 6h;
833 propan-2-ol/dichloromethane, 4/1, v/v, 250mL, 6h) to remove interstitial oil and the
834 residue dried (overnight, 70°C) before acidification by heating (70°C, overnight) in a
835 capped and sealed vial with hydrochloric acid (3 mL) and cyclohexane (3 mL). The
836 acidified organic fraction was recovered by extraction into diethylether (DEE; 3 x 5 mL)
837 by mixing (vortex 10 s) and centrifugation (2500 rpm/3 min). Solvent was removed from

838 the decanted supernatant under blow-down (N_2 , $70^\circ C$) prior to dilution in DEE/0.1%
839 ammonia (8 mL), loading on a pre-conditioned (1% aqueous ammonia, 20 mL; water, 20
840 mL; DEE, 10 mL) SAX solid phase extraction cartridge (Sigma-Aldrich Company Ltd.,
841 Dorset, UK; DSC-SAX, 12 mL, 2 g) and sequentially eluting the cartridge with 20 mL
842 volumes of DEE, dichloromethane and DEE/2% formic acid (FA). Solvent was removed
843 from the DEE/2% FA fraction ('acid fraction') under blow-down (N_2 , $70^\circ C$) and an
844 aliquot per-trimethylsilylated with BSTFA/1% TMCS (Sigma-Aldrich Company Ltd.,
845 UK; ca. 50 μL , $70^\circ C$, 1 hr) before dilution in cyclohexane for analysis using high
846 temperature gas chromatography (HTGC; Fig. SX1), or per-methylation for infusion
847 electrospray ionization/mass spectrometry (ESI-MS; Fig. SX2). An aliquot of the isolated
848 acid fraction was diluted in DEE for infrared spectroscopy (Fig. SX3).

849

850 The isolated acid fraction was reduced to alcohols by treatment with lithium aluminum
851 hydride ($LithAlH_4$; Sigma-Aldrich Company Ltd., UK; 1M in DEE). Dried acid fraction
852 was dissolved in a small volume (ca. 1 mL) dry DEE (sodium wire) and transferred with
853 washings to a small three-neck flask with Teflon flea and fitted with a Subaseal, calcium
854 chloride drying tube condenser and a glass stopper, all over a magnetic stirring block.
855 $LithAlH_4$ solution (ca. 3 mL) was pumped into the flask under nitrogen through the
856 Subaseal whilst stirring, additional dry DEE (ca. 5mL) was added through the condenser
857 to break up formed solids, before placing a bowl of warm water under the flask for 10
858 minutes. After the reaction vessel had cooled, wet DEE (prepared by mixing DEE and
859 water in separating funnel and drawing off aqueous phase) was added (10 mL, drop-wise
860 at first) to hydrolyse unreacted hydrides, followed by drop-wise addition of sulphuric

861 acid (10% aqueous; ca. 1 mL) to destroy remaining LiAlH_4 . The contents of the flask
862 were transferred with washings (ca. 3 mL, 10% $\text{H}_2\text{SO}_{4(\text{aq})}$) to a separating funnel and the
863 organic phase ('alcohol fraction') collected after washing with water (3 x 3 mL). Solvent
864 was removed from the alcohol fraction by blow-down (N_2 , 70°C) and aliquots prepared
865 for HTGC, ESI-MS and IR spectroscopy as above. All solvents were HPLC grade
866 (Rathburn Chemicals Ltd., Walkerburn, UK or Fisher Scientific UK Ltd., Loughborough,
867 UK) or LC/MS grade (Chromasolv®; Sigma-Aldrich Company Ltd., Dorset, UK), water
868 was Elga Maxima (18.2 mΩ; Elga Ltd., Buckinghamshire, UK).

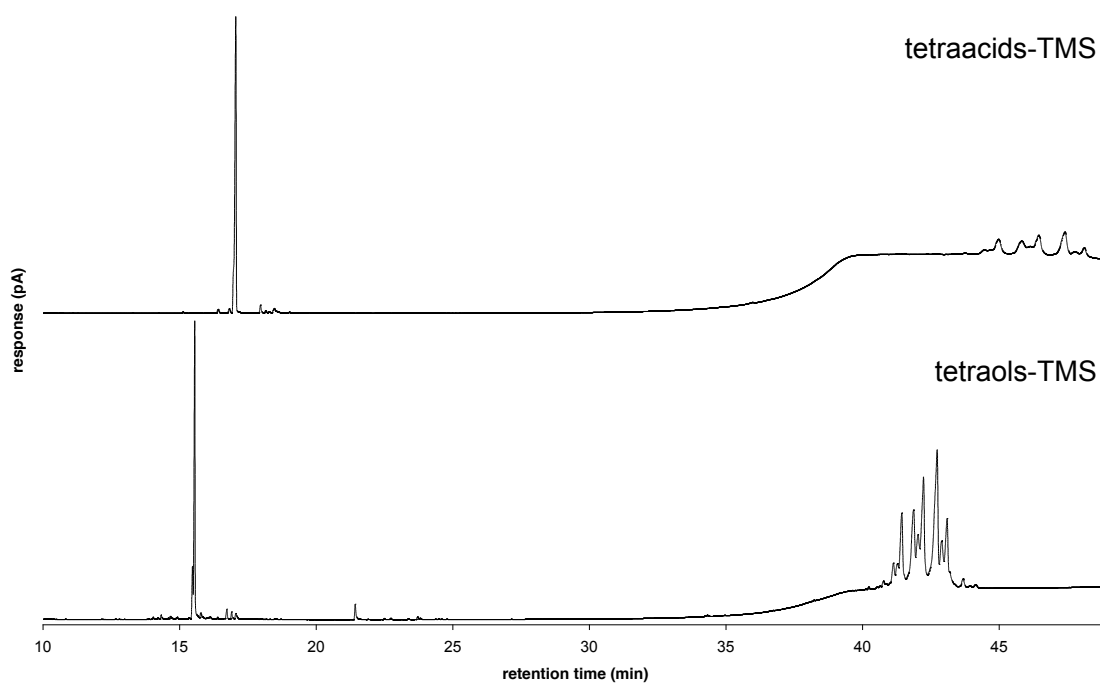
869

870 Reduction of the tetraacids to tetrols was monitored using HTGC (Fig. SX1), ESI-MS
871 (Fig. SX4 and SX5) and IR spectroscopy (Fig. SX3). The HTGC system comprised an
872 Agilent 6890 GC fitted with cool-on-column inlet ($+3^\circ\text{C}$ track oven mode; 0.5 μL manual
873 injection), flame ionization detector (435°C) and Varian VF-5ht Ultimet column (15 m
874 x 0.25 mm x 0.1 μm) with helium carrier gas (1 ml min^{-1} , constant flow) and oven
875 programme from 40 – 430°C at $10^\circ\text{C min}^{-1}$ with 10 min hold.

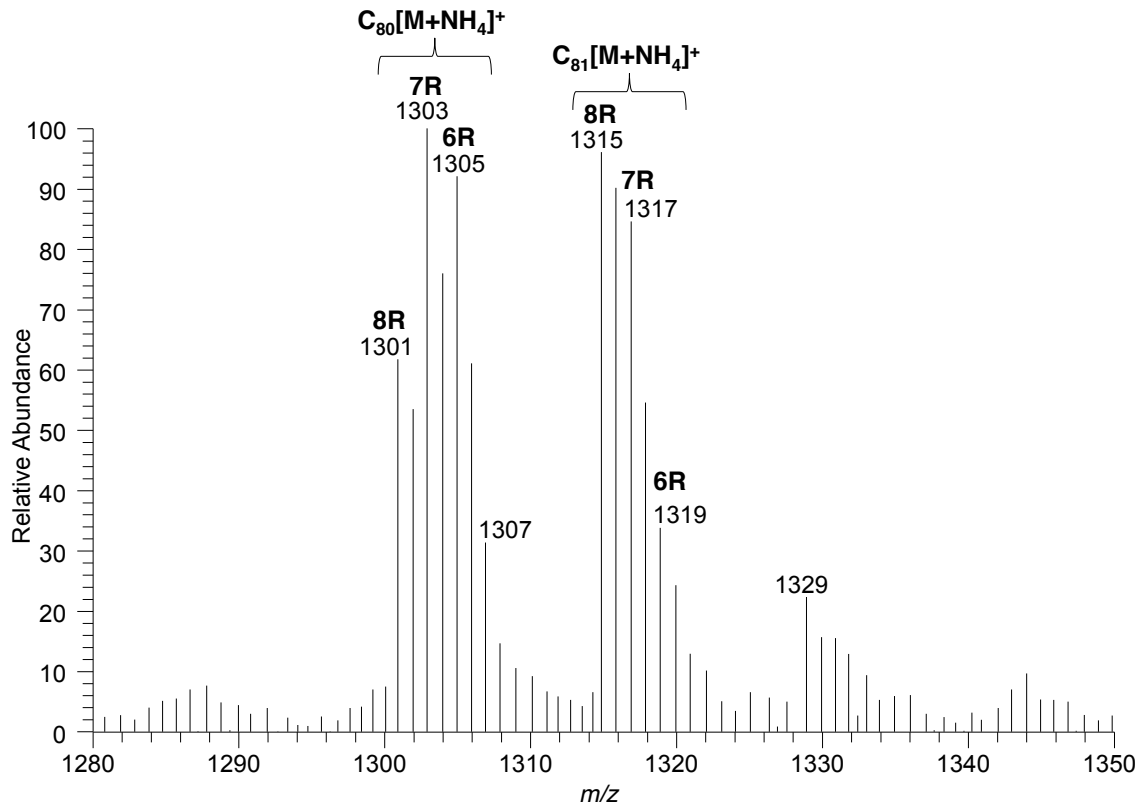
876

877 Infusion ESI-MS was carried out in positive ionization mode using a Finnigan Mat
878 LCQ™ (ThermoFinnigan, San Jose, CA, USA) with ESI interface. Samples were diluted
879 in propan-2-ol/10mM ammonium acetate and infused at 3 $\mu\text{L min}^{-1}$ with a Hamilton
880 (Reno, CA, USA) 1725N (250 μL) syringe using the built-in syringe pump. Mass spectral
881 data were acquired (and averaged over 1 minute) and processed using Xcalibur software.
882 Typical instrument parameters were: source voltage (\pm) 4.5 kV; capillary voltage (\pm) 60
883 V; capillary temperature 200°C ; nitrogen sheath gas flow rate 24 (arbitrary units).

884 Instrumental parameters were optimised on the most abundant ion using the autotune
885 function.
886
887 Infrared spectroscopy was carried out using a Bruker Alpha Platinum ATR (Bruker Optik
888 GmbH, Ettlingen, Germany) by measuring 32 sample scans (resolution 4 cm^{-1} ;
889 transmittance) and recording data between $4000 - 375\text{ cm}^{-1}$. Background comprised 32
890 scans without sample.
891



892
893 Figure SX1. High temperature gas chromatograms of trimethylsilylated tetraacids
894 obtained from an oilfield deposit (upper) and lower the trimethylsilylated tetraols
895 obtained following LiAlH_4 reduction (lower).
896



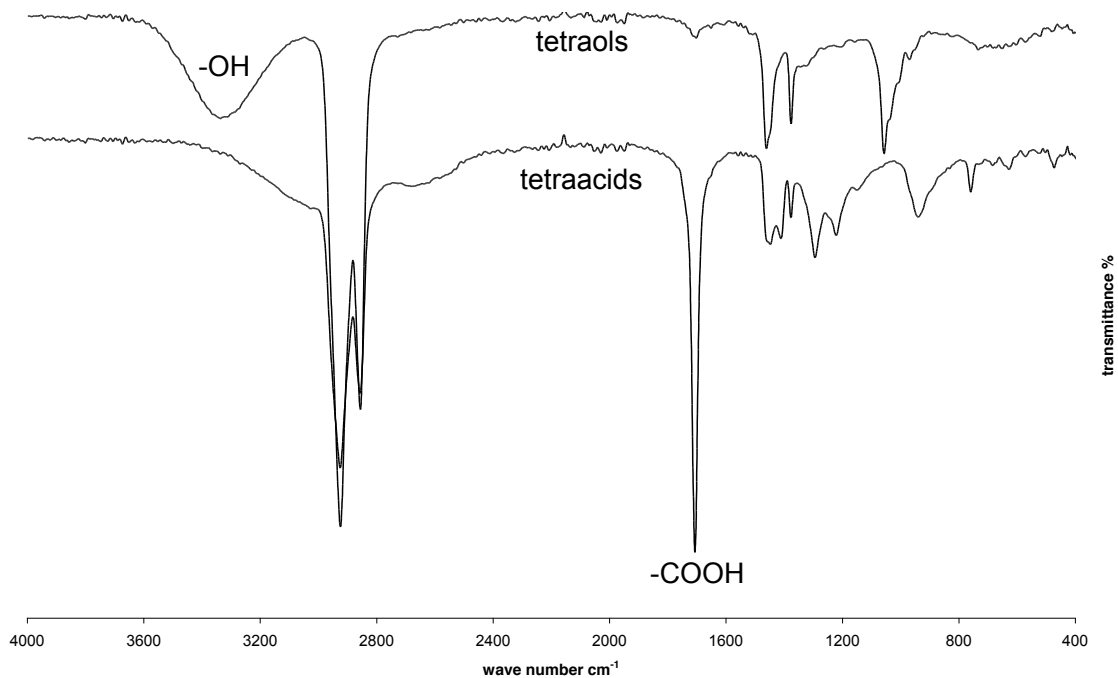
897

898 Figure SX2. Averaged mass spectrum (18.6 – 19.6 min) from Infusion ESI-MS of per-
 899 methylated esters of tetraacids obtained from an oilfield deposit (nR refers to the number
 900 of cyclopentyl rings in the molecule).

901

902

903



904

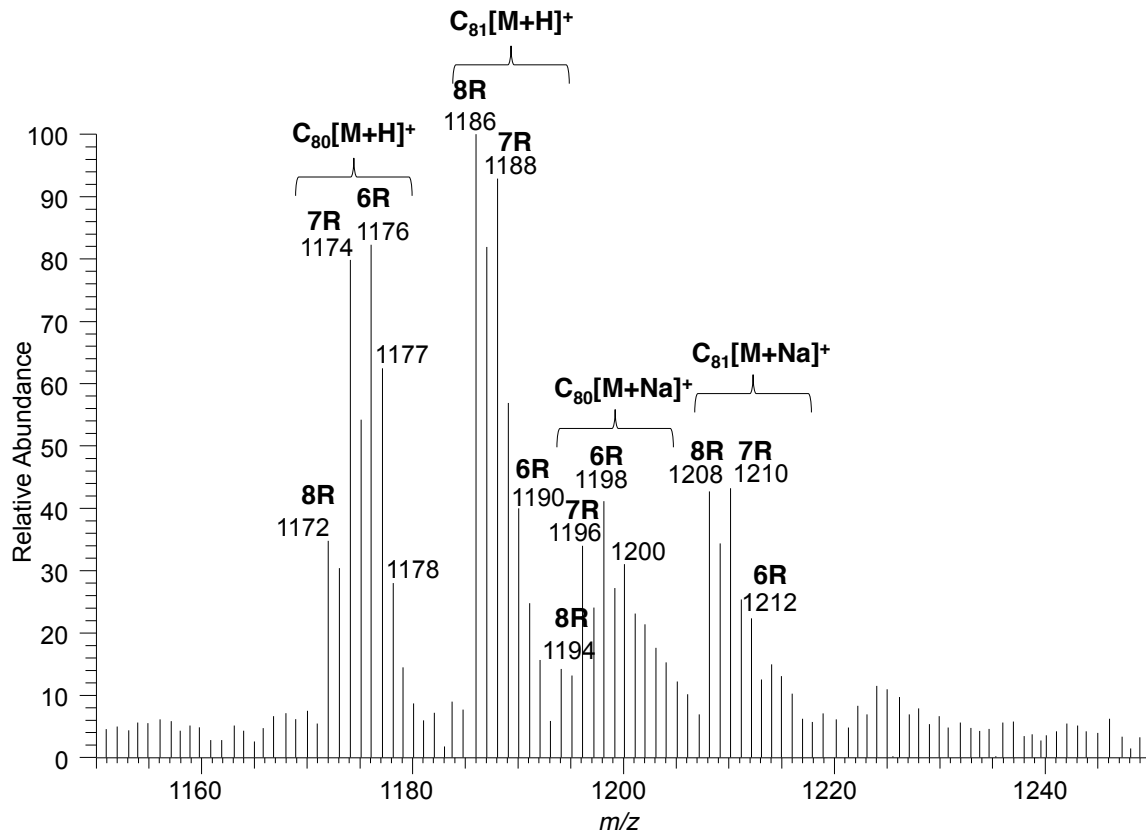
905 Figure SX3. FTIR transmittance spectra of tetraacids isolated from an oilfield deposit

906 (lower) and tetraols produced from the tetraacids by LiAlH_4 reduction (upper).

907

908

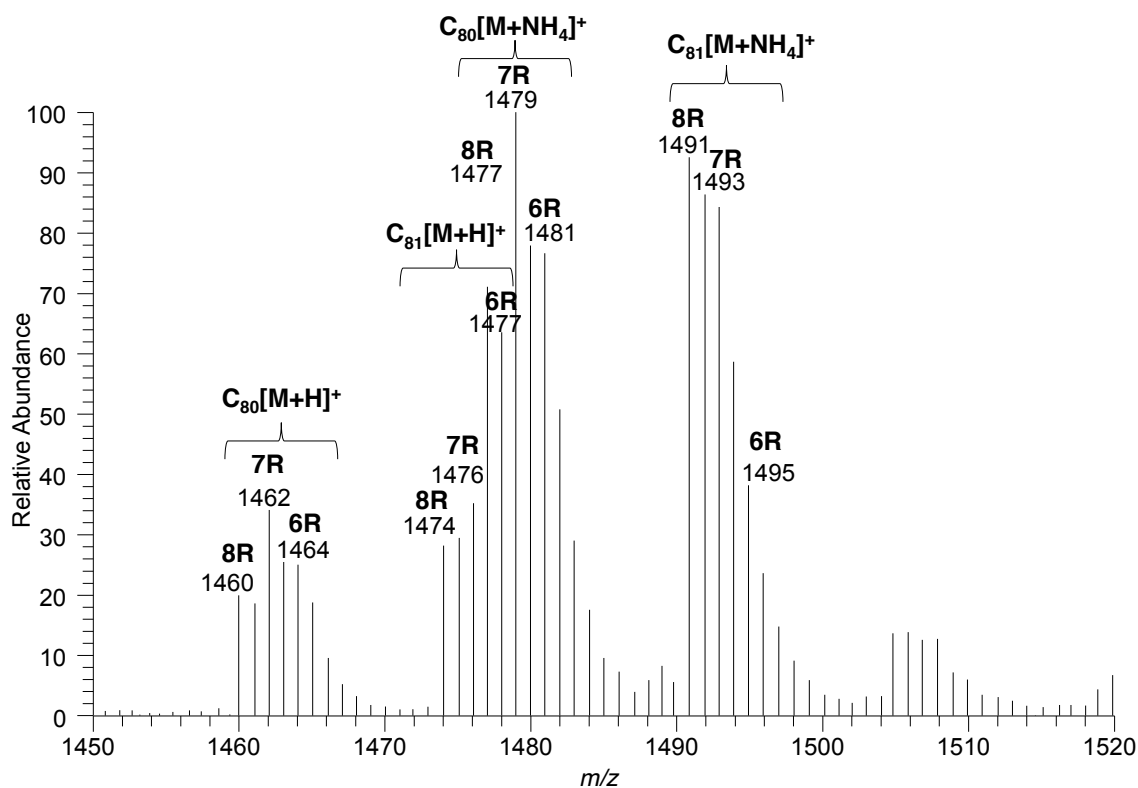
909



910

911 Figure SX4. Infusion ESI-MS of underivatized tetraols obtained from the LithAl
 912 reduction of tetraacids from an oilfield deposit (nR refers to the number of cyclopentyl
 913 rings in the molecule).

914



915

916 Figure SX5. Infusion electrospray ionization (+ve) mass spectrum of per-

917 trimethylsilylated tetraols obtained from the LithAl reduction of tetraacids from an

918 oilfield deposit (nR refers to the number of cyclopentyl rings in the molecule).

919

920

921 3. Acid hydrolysis of GDGT-0 standard

922 GDGT-0 standard was isolated with a semi-preparative LC protocol (as described in Zhu

923 et al., 2014) from acid-hydrolyzed biomass of *Archaeoglobus fulgidus*. Strong acid

924 hydrolysis was then performed with 10% methanolic HCl and GDGT-0 standard under

925 70 °C for 96 hours. After dried with a N₂ flow the treated sample was dissolved in *n*-

926 hexane for NPLC-APCI-MS analysis.

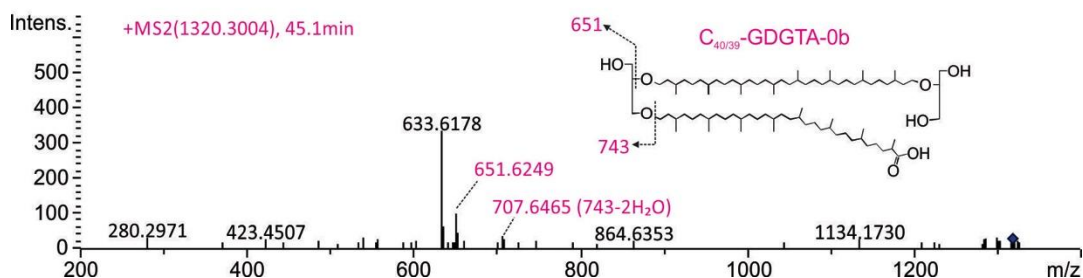
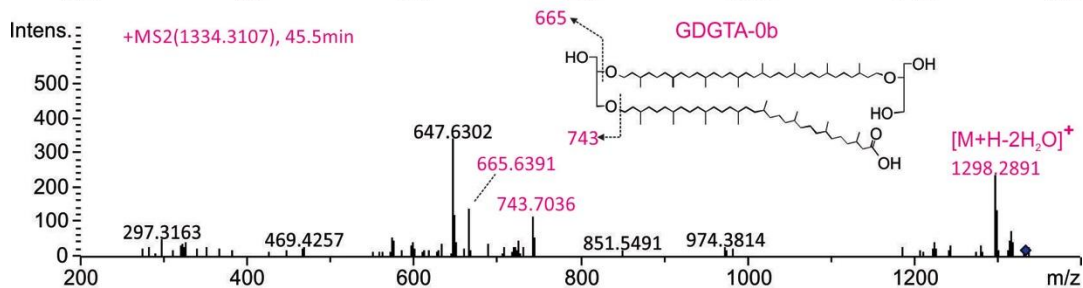
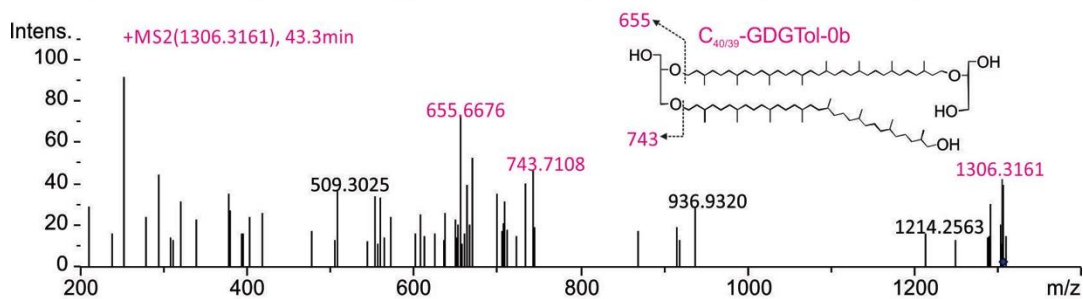
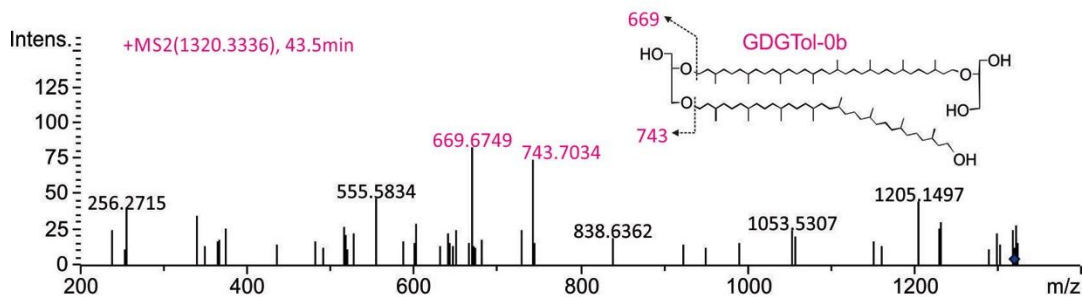
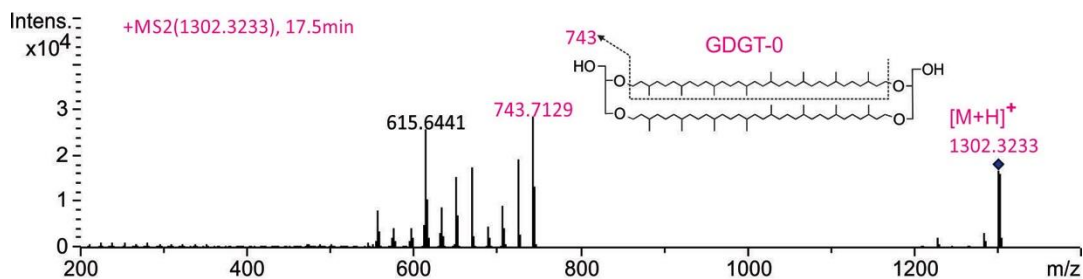
927

928

929 **Reference:**

930 Zhu, C., Meador, T.B., Dummann, W., Hinrichs, K.-U., 2014. Identification of unusual
931 butanetriol dialkyl glycerol tetraether and pentanetriol dialkyl glycerol tetraether lipids in
932 marine sediments. *Rapid Commun. Mass Spectrom.* 28, 332–338.

933

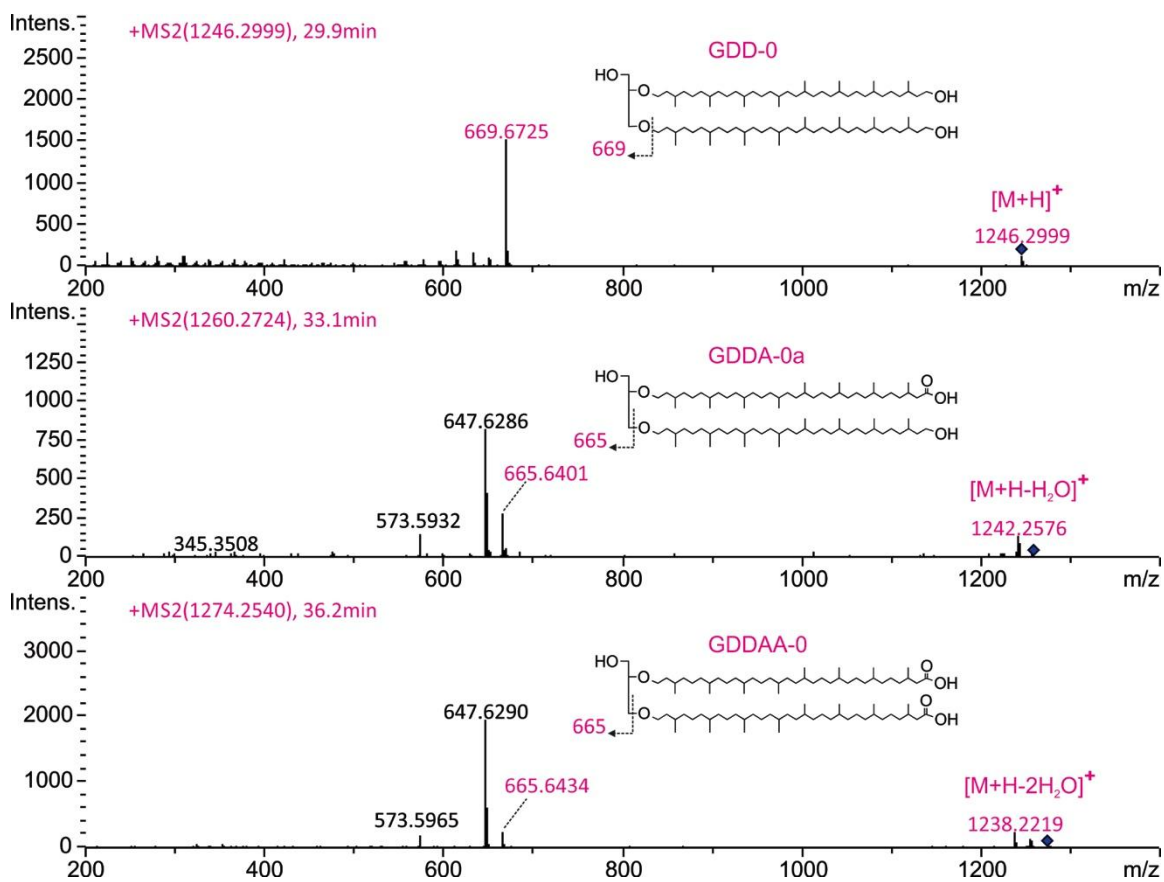


934

935

936 **Figure S1a.** MS² fragmentation patterns supporting the identification of GDGT-0,
 937 GDGTol-0 and GDGTA-0 in Fig. 1a, and C_{40/39}-GDGTol-0 and C_{40/39}-GDGTA-0 in Fig.
 938 3e.

939



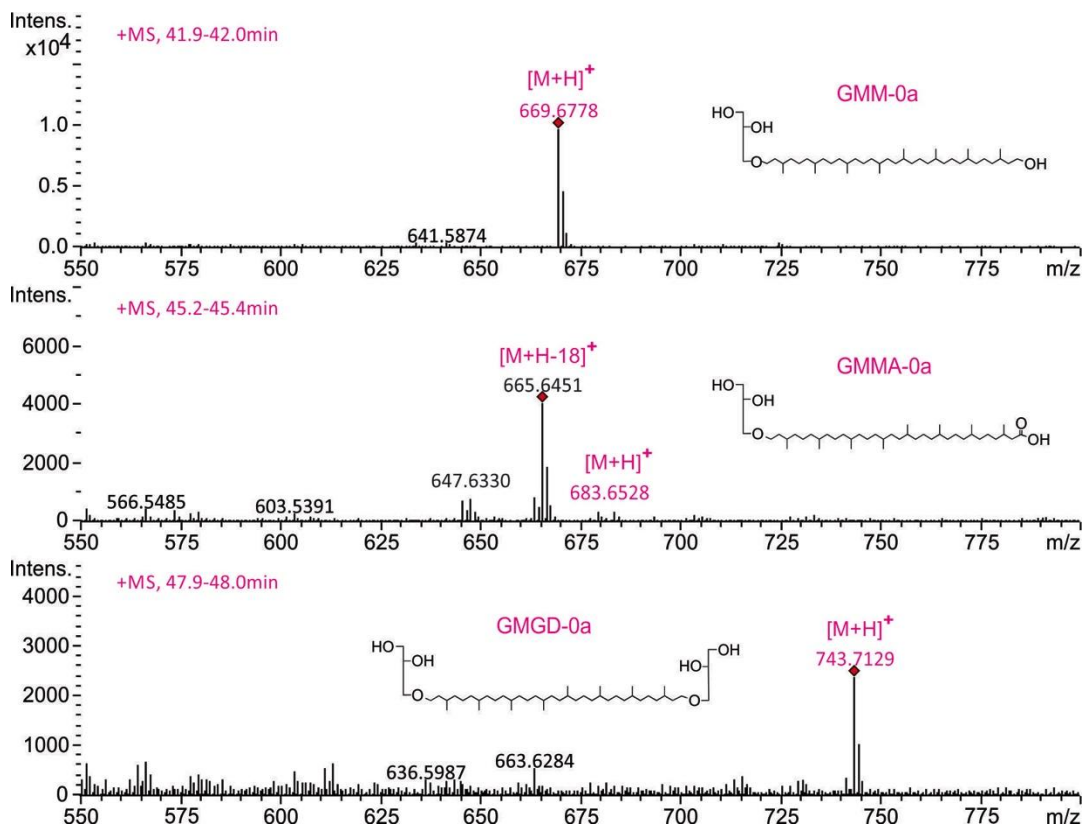
940

941

942 **Figure S1b.** MS² fragmentation patterns supporting the identification of GDD-0, GDDA-
943 0 and GDDAA-0 in Fig. 1a.

944

945



946

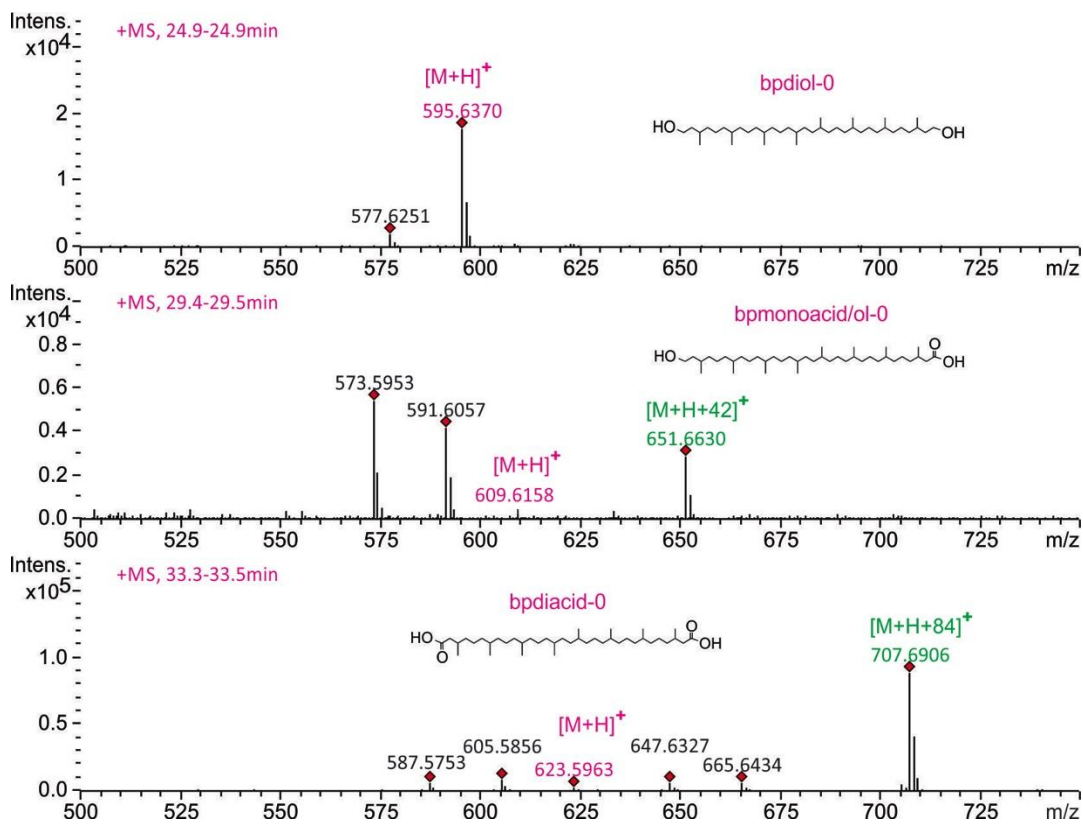
947

948 **Figure S1c.** MS¹ ions supporting the identification of GMM-0, GMMA-0 and GMGD-0
 949 in Fig. 1b.

950

951

952



953

954 **Figure S1d.** MS¹ ions supporting the identification of bpdial-0, bpmmonoacid/ol-0 and
 955 bpdiaacid-0 in Fig. 1b.

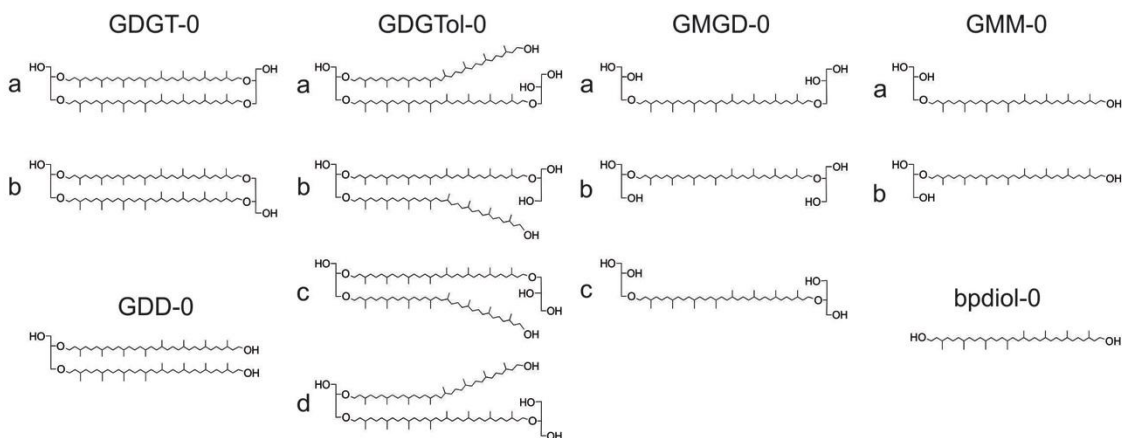
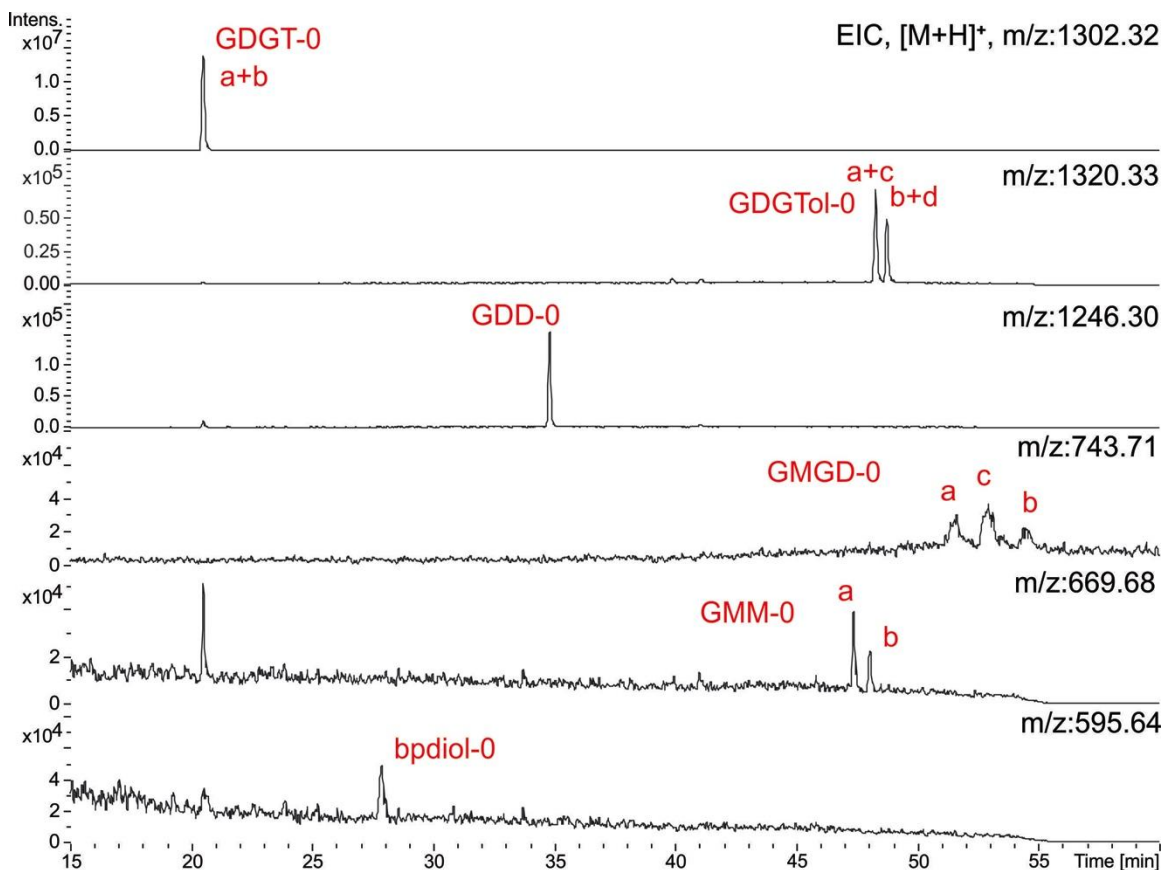
956

957

958

959

960



961

962

963 **Figure S2**

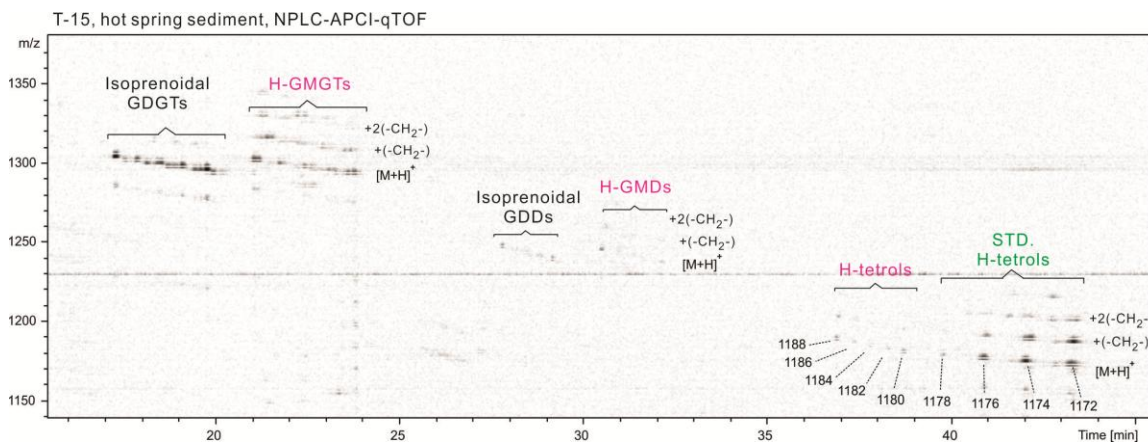
964 Major hydroxyl derivatives released from GDGT-0 by chemical degradation, a mild ether
 965 cleavage conducted by adding 1000ng GDGT-0 into 1mL of 10% HCl in methanol, and

966 heated to 70 °C for 96 hours. The composition of GMGDs indicated a nearly 1:1 mixture
967 of parallel and anti-parallel GDGT-0.

968

969

970



971

972 **Figure S3**

973 Density maps of NPLC-APCI-qTOF showing the occurrence of H-GMGTs and their
974 degradation derivatives in the hot spring sediment, T-15. The identification of H-tetrols
975 are confirmed by their similar chromatographic behavior with added standards (green
976 color text).

977

978

979

Compounds	Abbreviation	Structural illustration	Distribution				
			Leg201-1227	Marmorito seep carbonate	Guaymas Basin 4568	Hot spring T-15	<i>N. maritimus</i> late stat. phase
glycerol dialkyl glycerol tetraether	GDGT		+	+	+	+	+
glycerol dialkyl glycerol triether alcohol	GDGTol		+	+	+	n.d.	+
glycerol dialkyl glycerol triether acid	GDGTA		+	+	n.d.	n.d.	n.d.
glycerol dibiphytanol diether	GDD		+	+	+	+	+
glycerol dibiphytanol diether monoacid	GDDA		+	+	+	n.d.	+
glycerol dibiphytanol diether diacid	GDDAA		n.d.	+	n.d.	n.d.	n.d.
glycerol monobiphytanyl glycerol diether	GMGD		+	+	+	n.d.	n.d.
glycerol monobiphytanol monoether	GMM		+	+	+	n.d.	n.d.
glycerol monobiphytanol monoether acid	GMMA		n.d.	+	n.d.	n.d.	n.d.
biphytanic diol	bpdiol		+	+	+	+	+
biphytanic monoacid	bpmonoacid/ol		+	+	n.d.	n.d.	n.d.
biphytanic diacid	bpdiacid		n.d.	+	n.d.	n.d.	n.d.
H-shaped glycerol monoalkyl glycerol tetraether	H-GMGT		+	+	+	+	n.d.
H-shaped glycerol monoalkyl diether	H-GMD		+	+	+	+	n.d.
H-shaped C ₈₀ tetrol	H-tetrol		+	+	+	+	n.d.
H-shaped C ₈₀ monoacid	H-monoacid		n.d.	n.d.	+	n.d.	n.d.
H-shaped C ₈₀ diacid	H-diacid		n.d.	n.d.	+	n.d.	n.d.
H-shaped C ₈₀ triacid	H-triacid		n.d.	n.d.	+	n.d.	n.d.
H-shaped C ₈₀ tetraacid	H-tetraacid		n.d.	n.d.	+	n.d.	n.d.

Figure

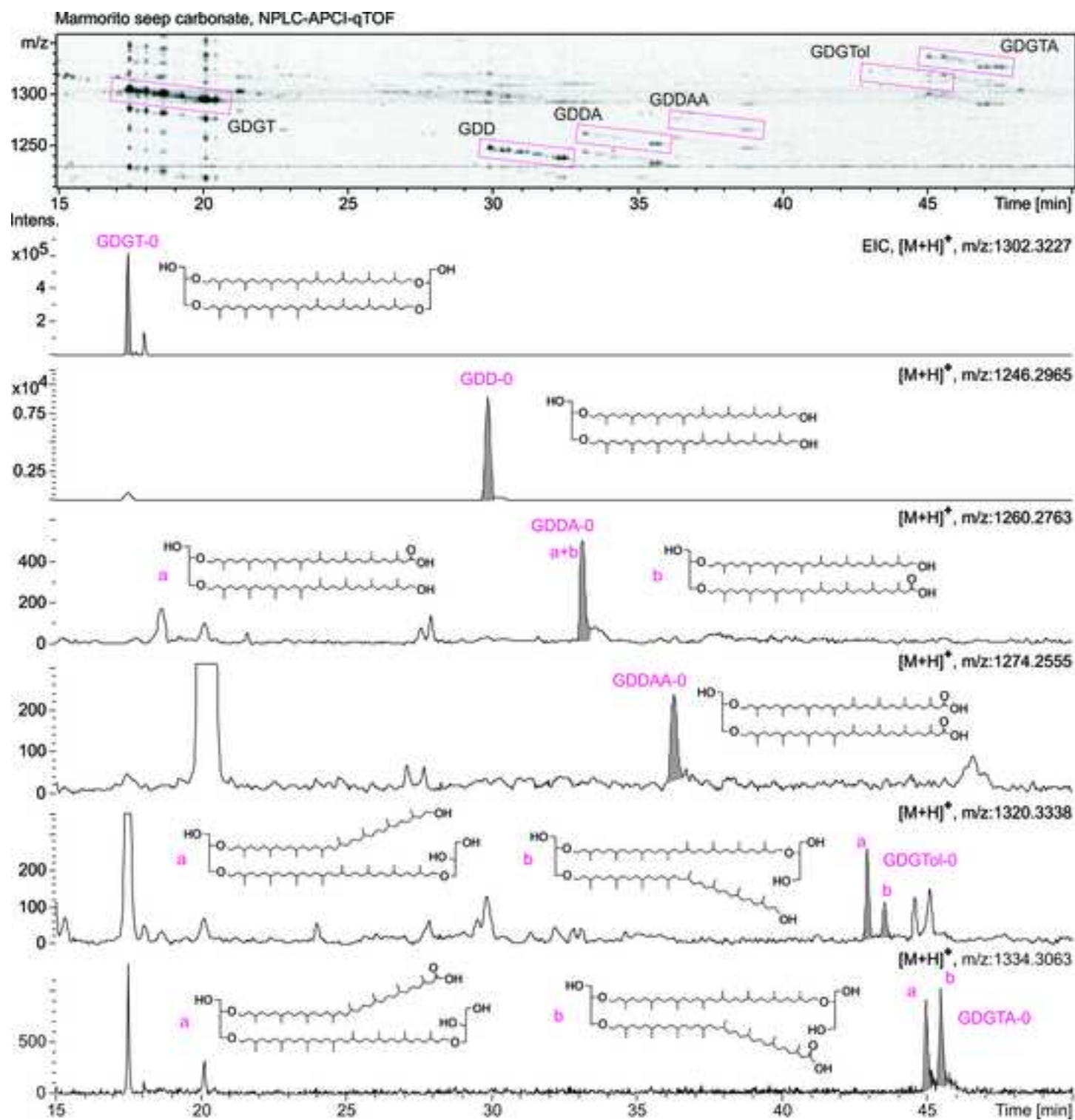
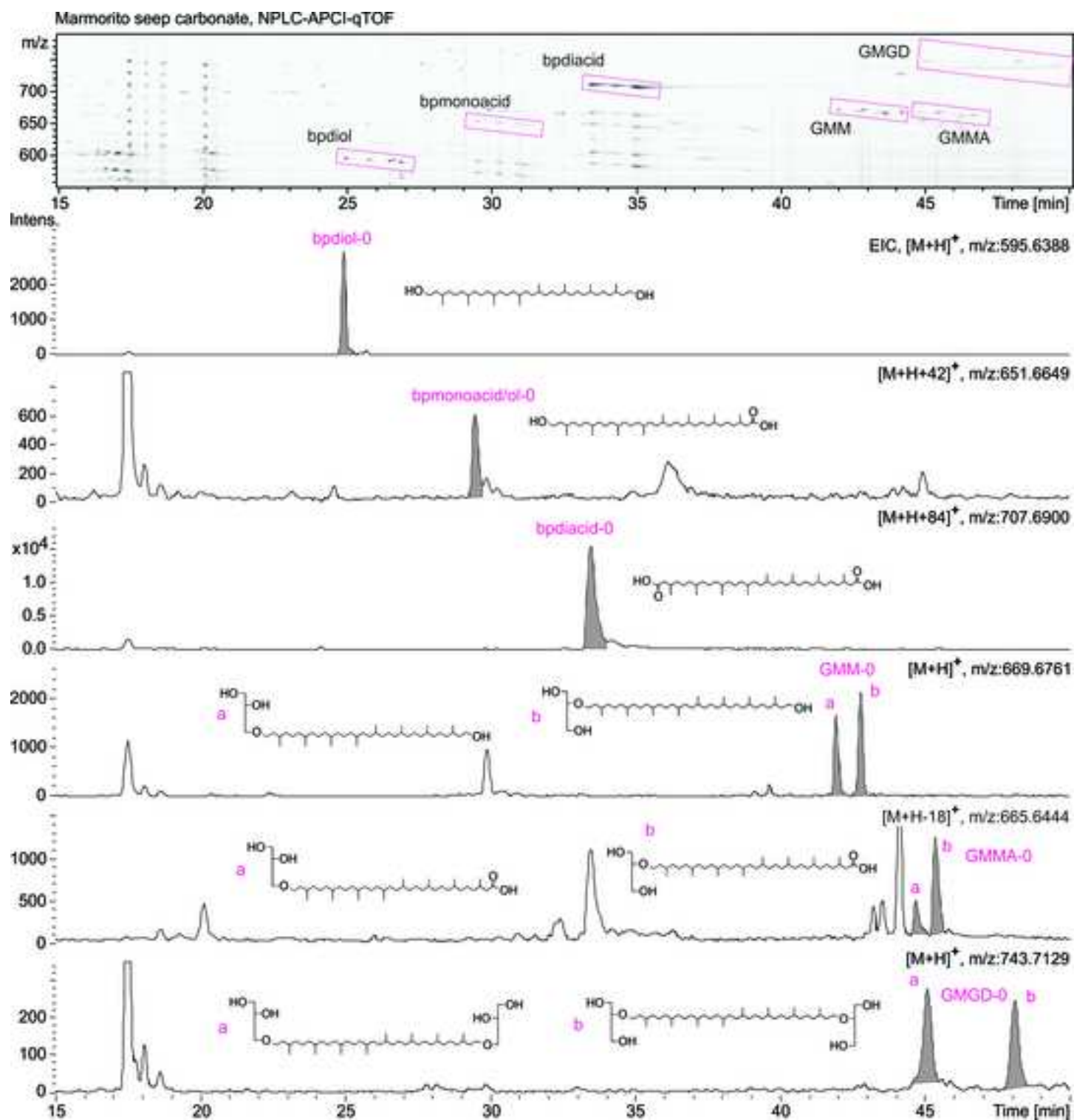
[Click here to download high resolution image](#)

Figure
[Click here to download high resolution image](#)



Figure

[Click here to download high resolution image](#)

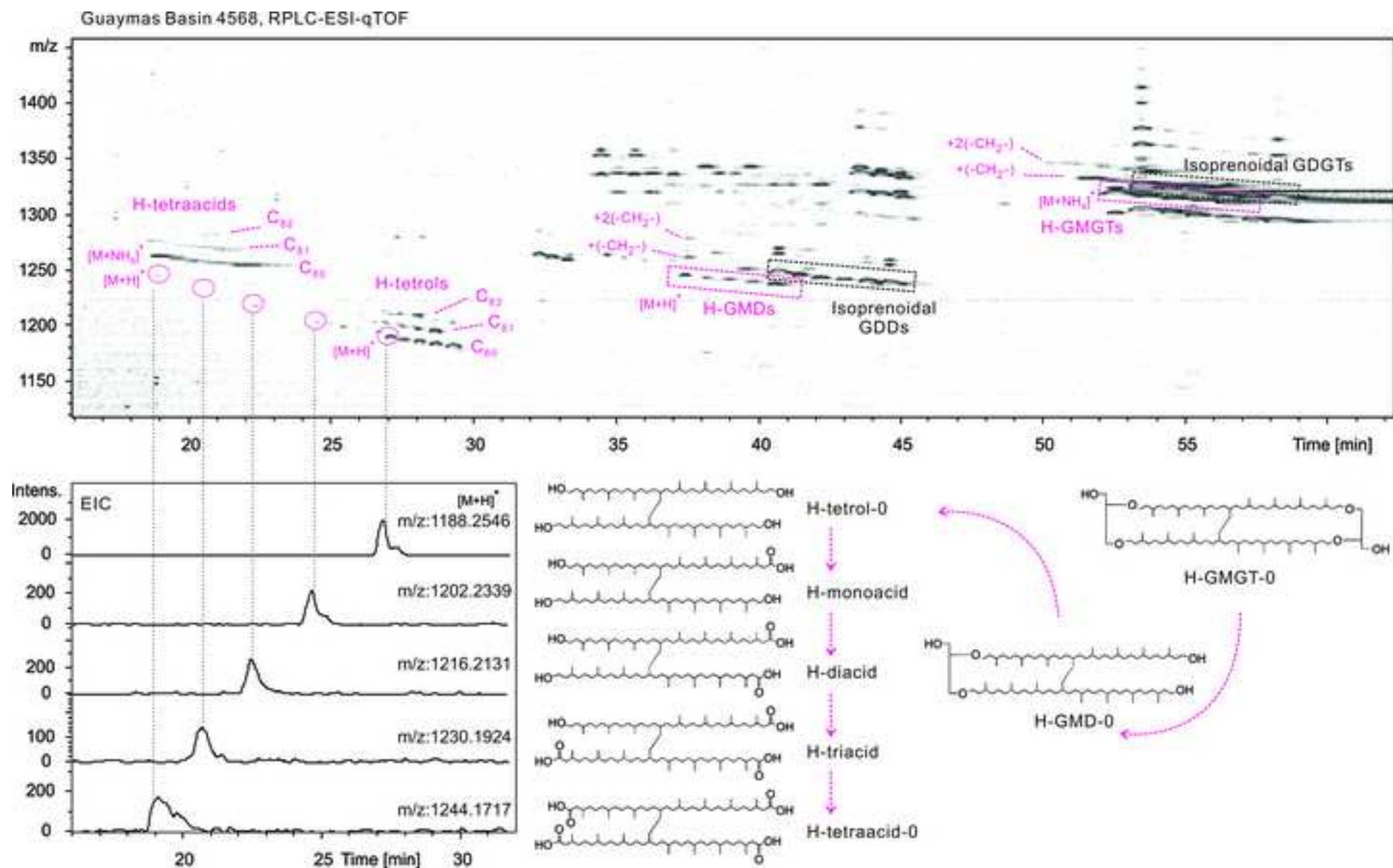


Figure
[Click here to download high resolution image](#)

Leg 201-1227, NPLC-APCI-qTOF

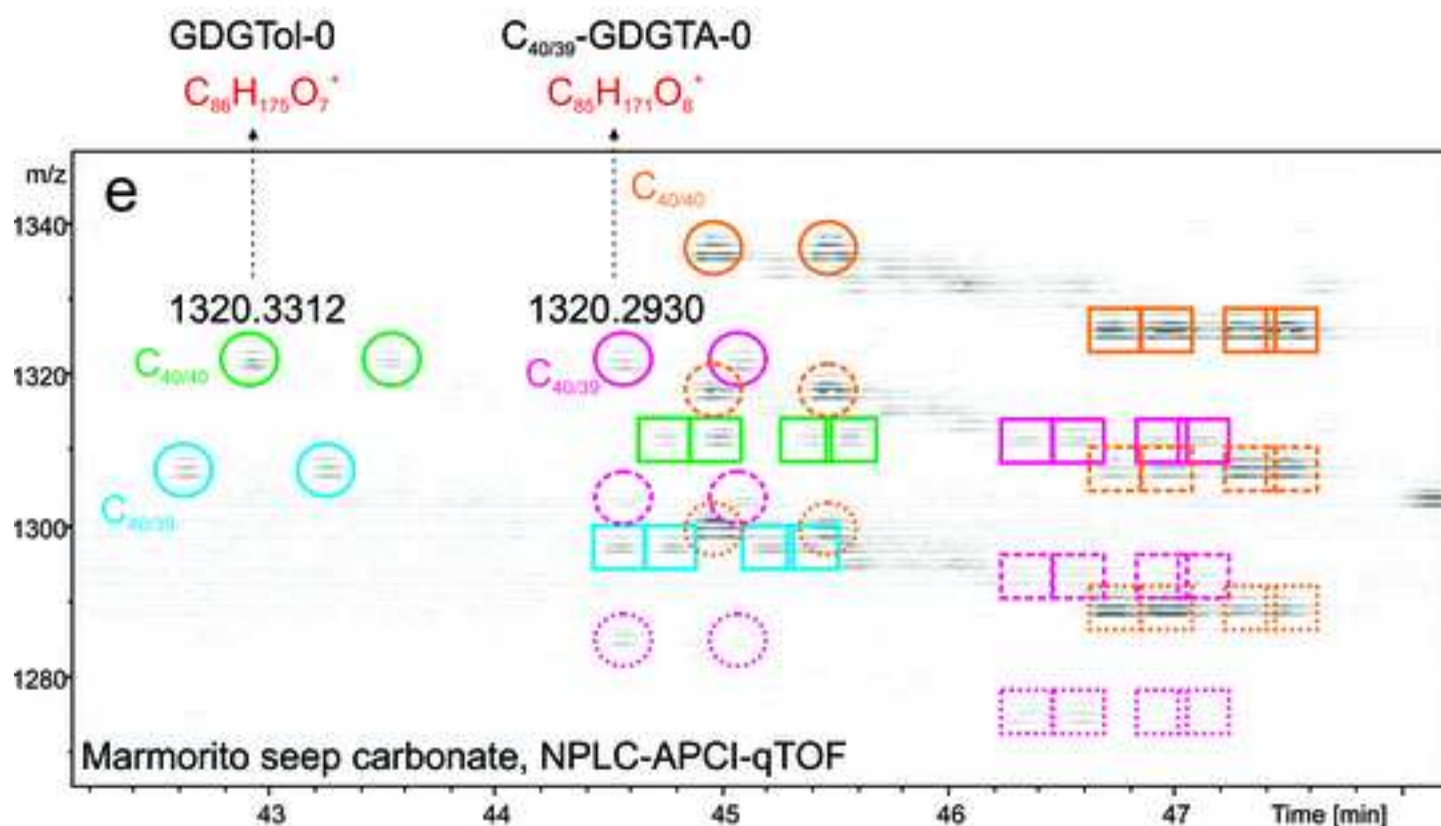
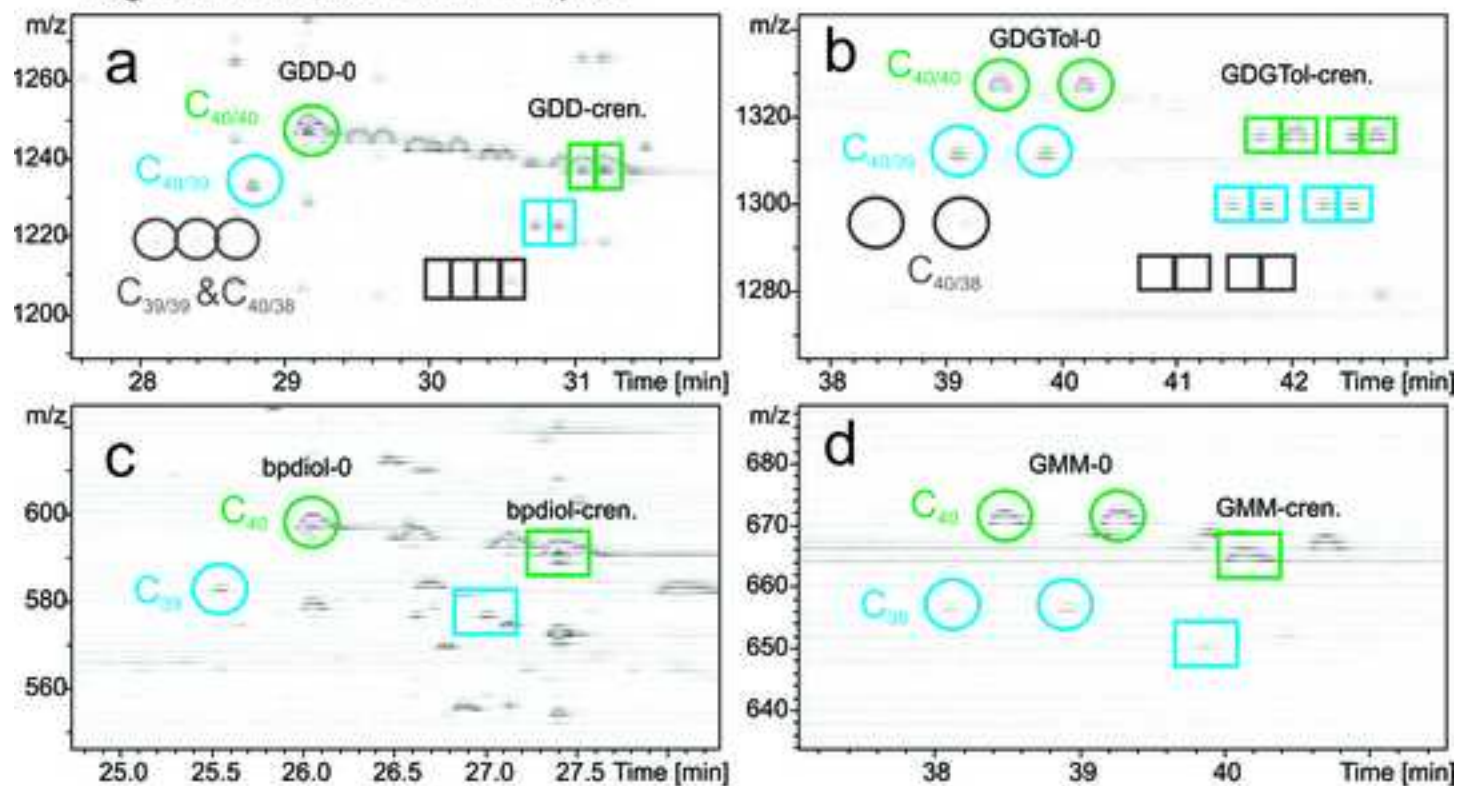
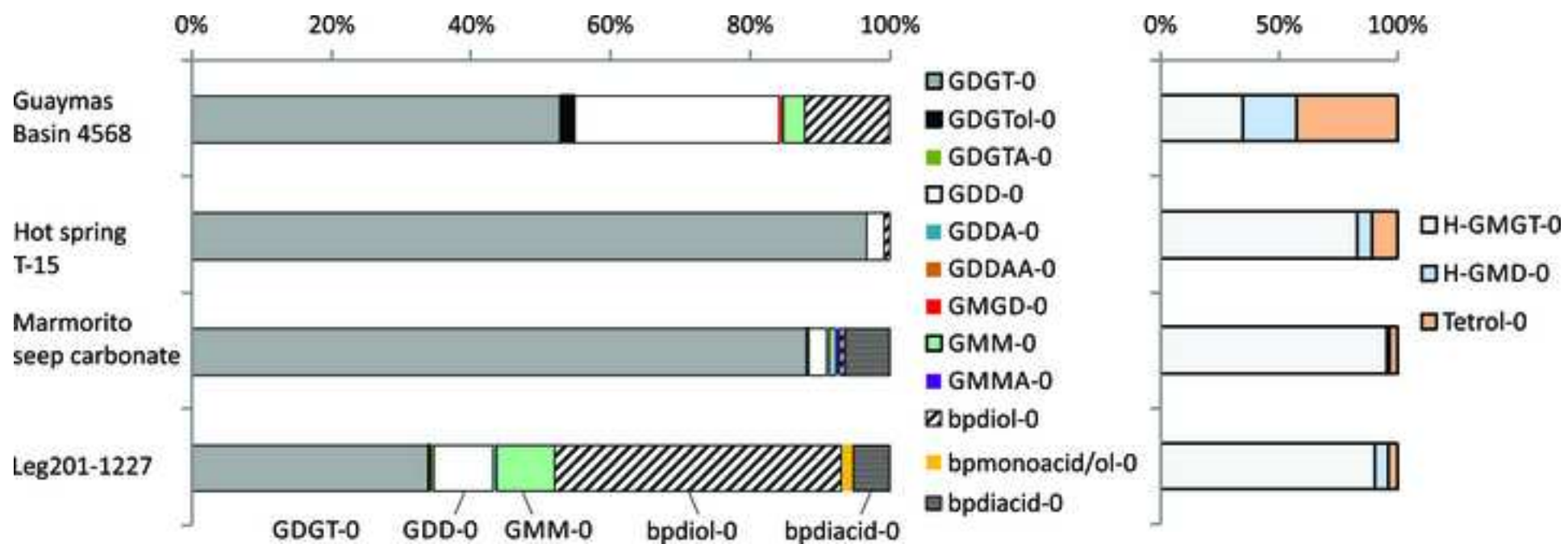


Figure
[Click here to download high resolution image](#)



Figure

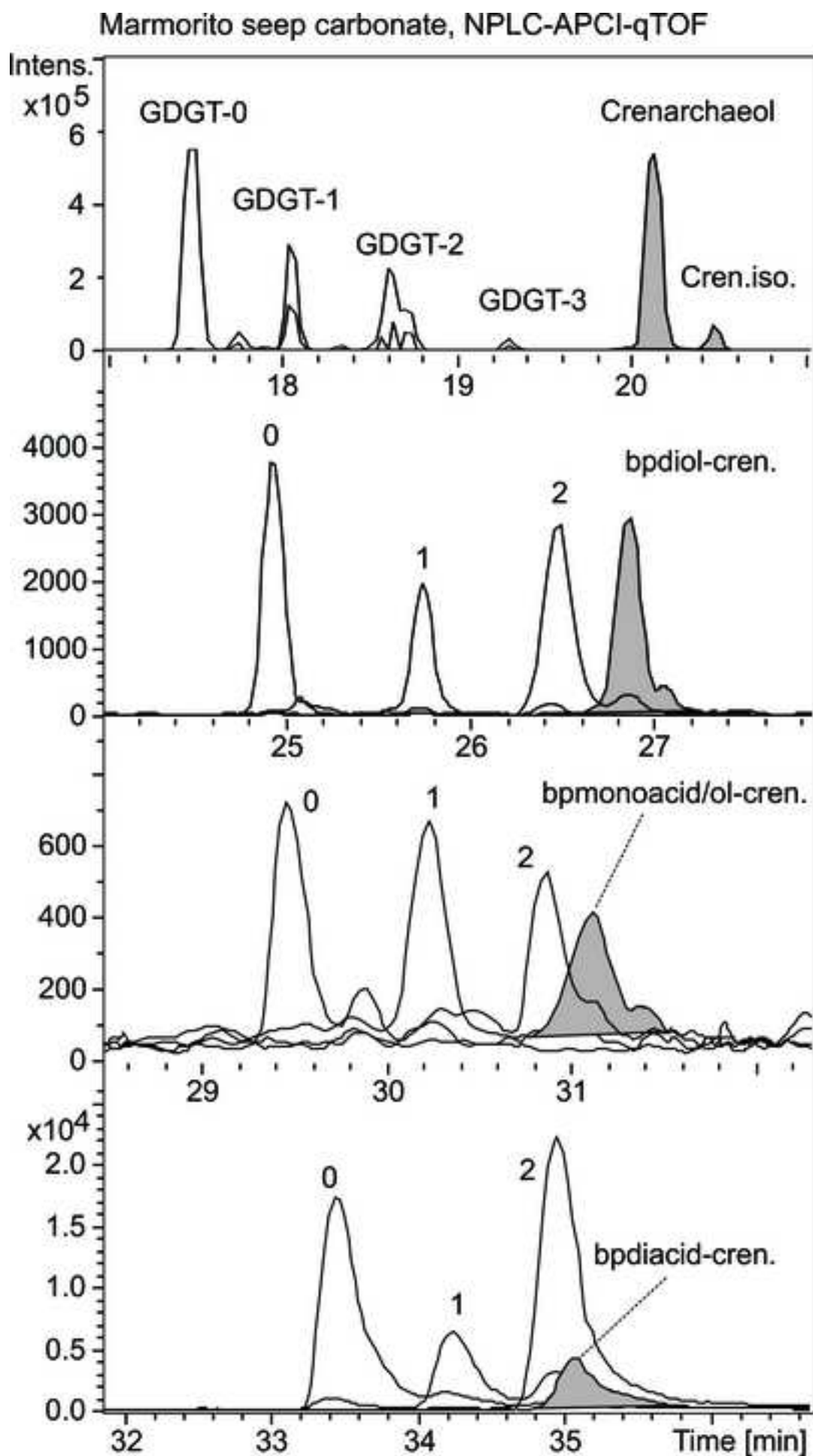
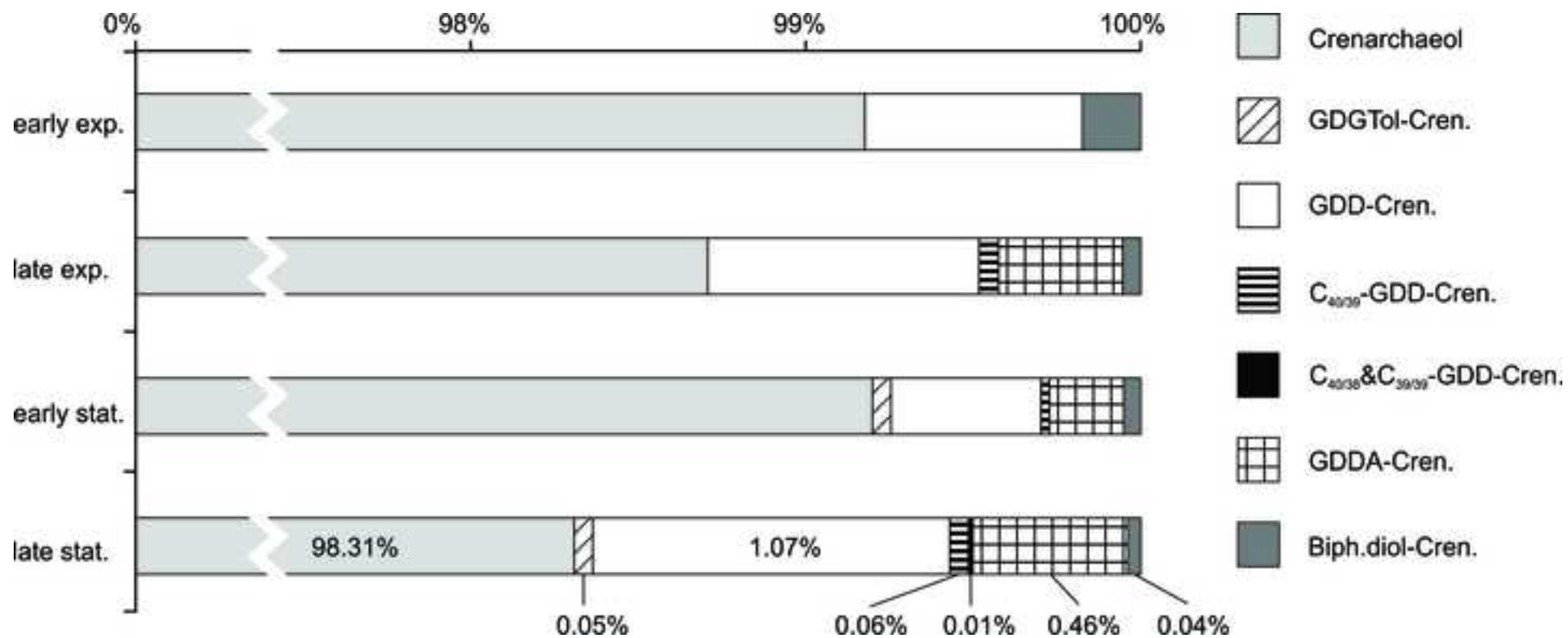
[Click here to download high resolution image](#)

Figure
[Click here to download high resolution image](#)



Figure

[Click here to download high resolution image](#)

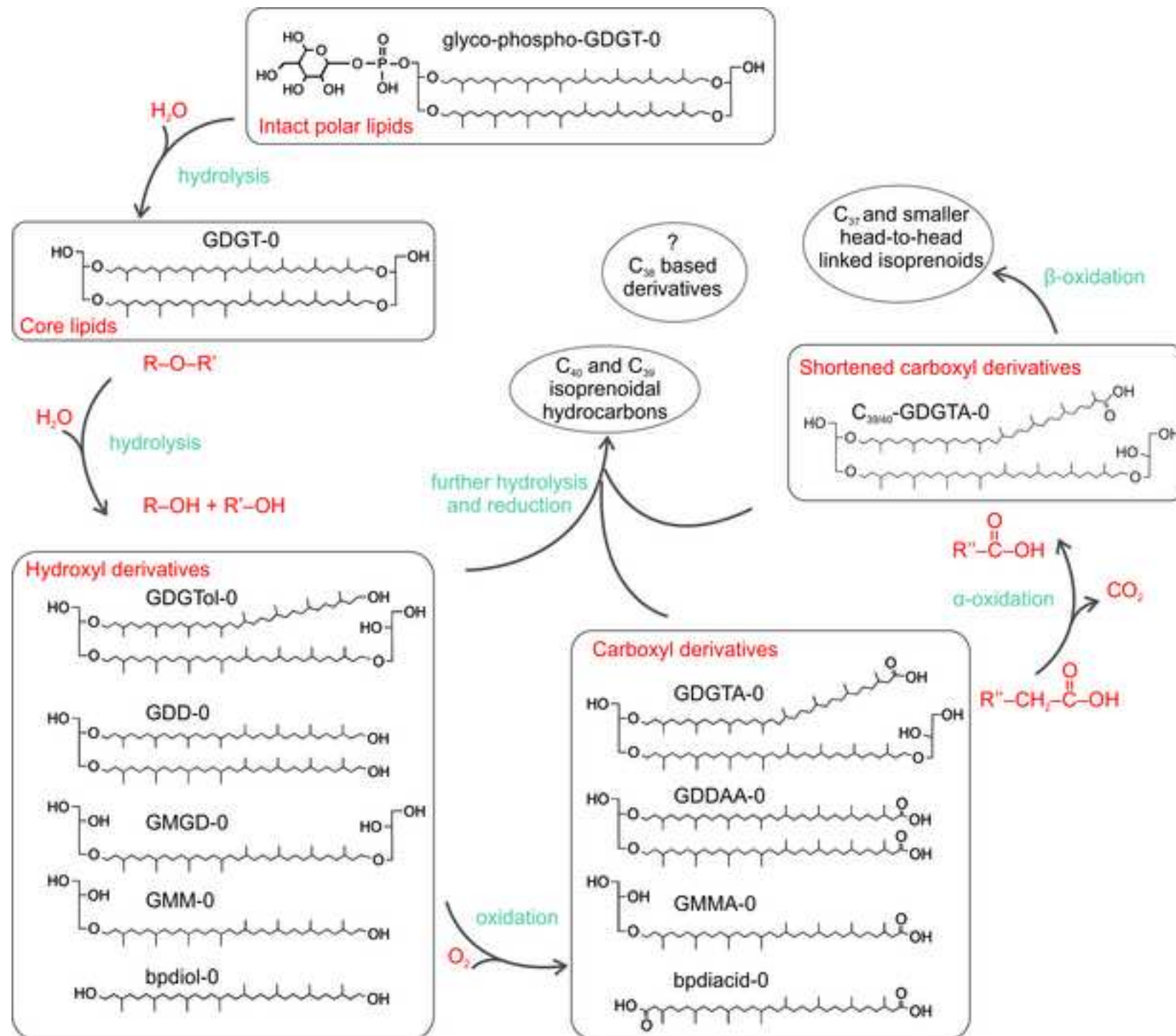
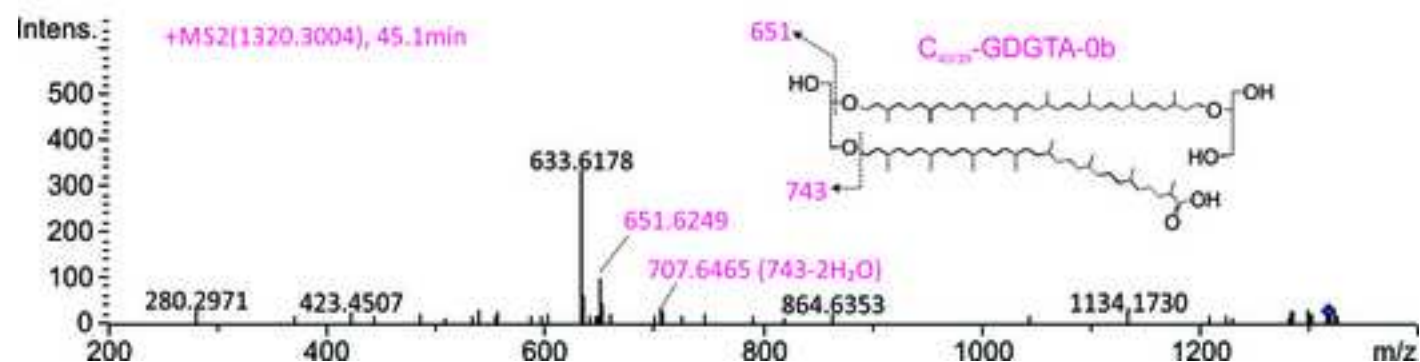
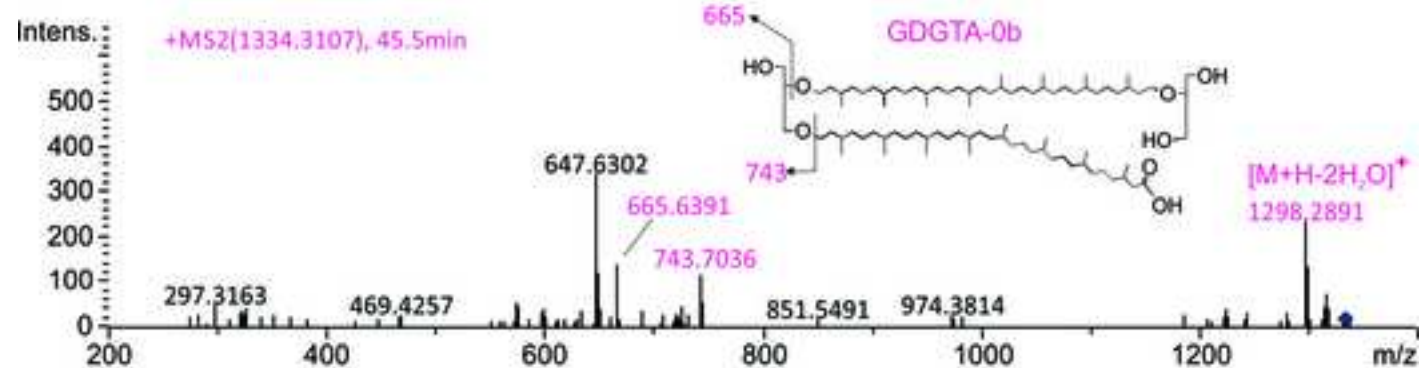
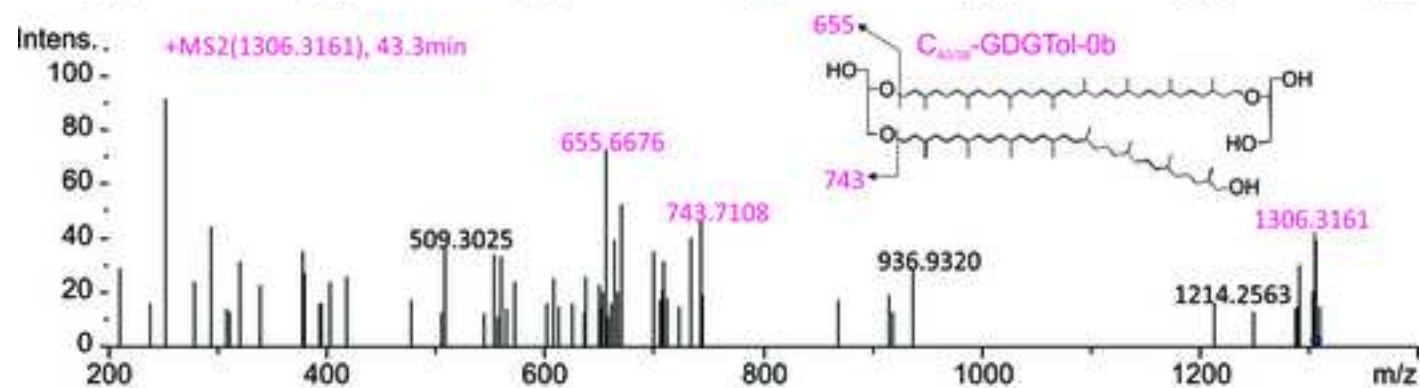
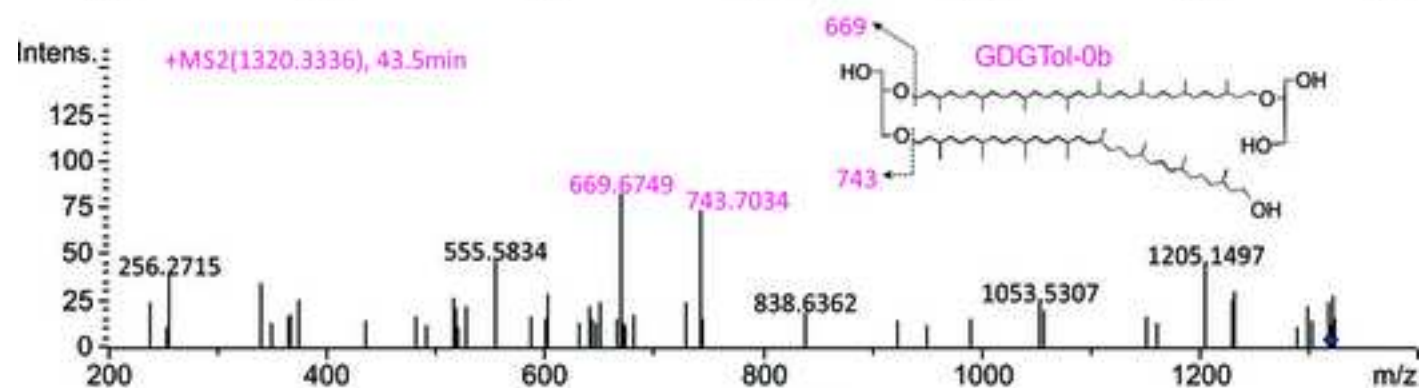
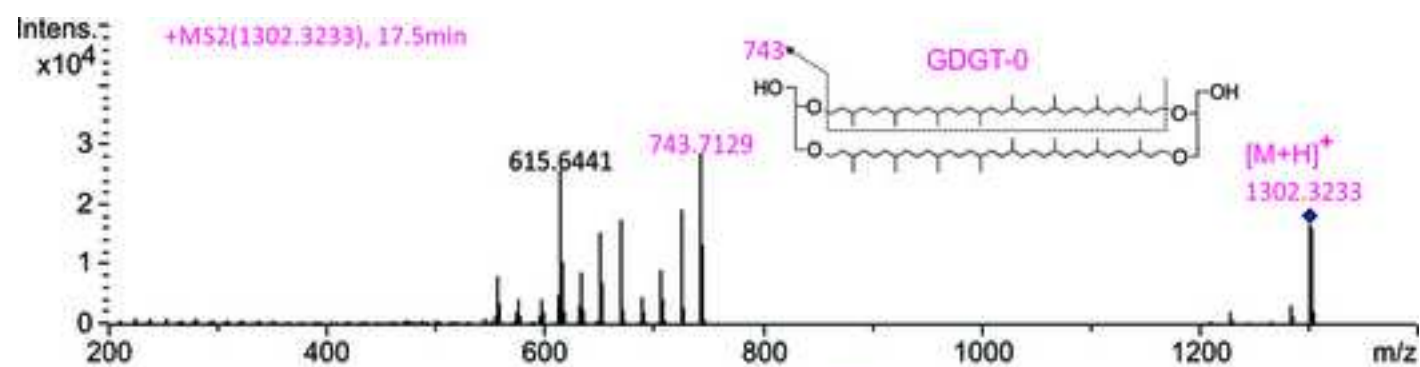
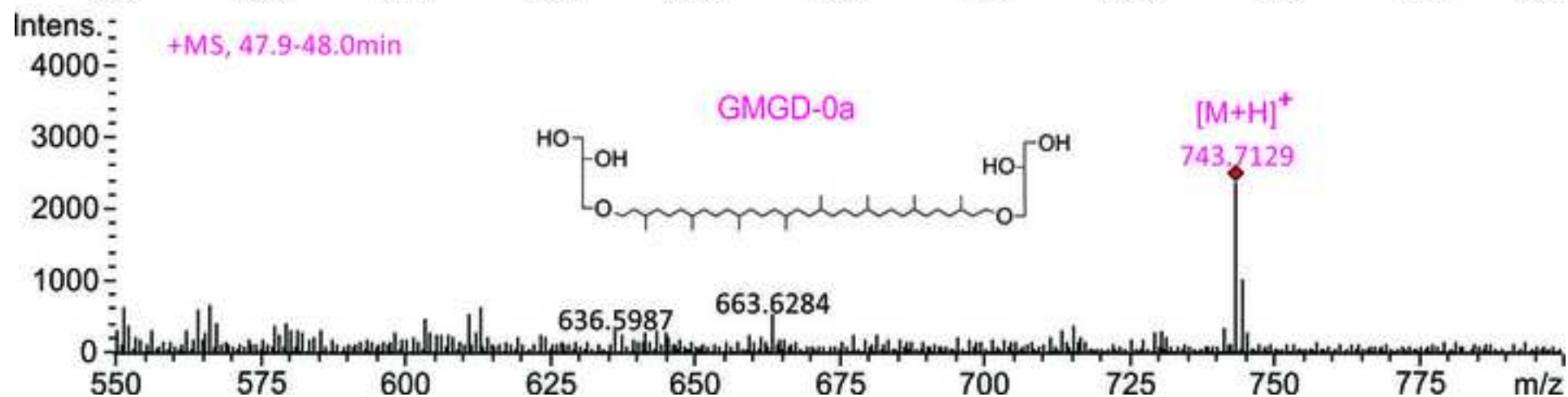
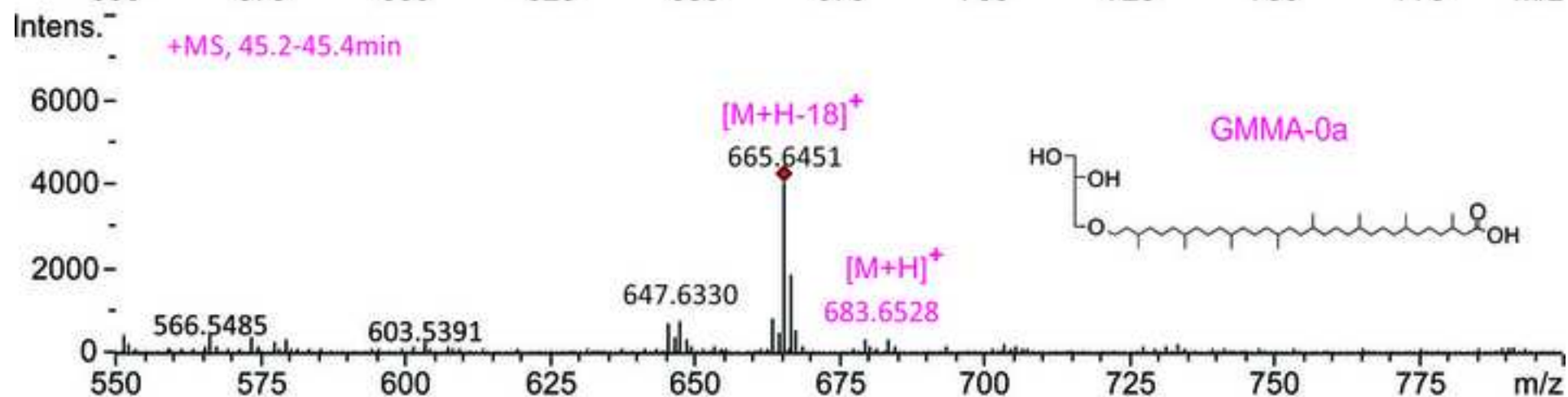
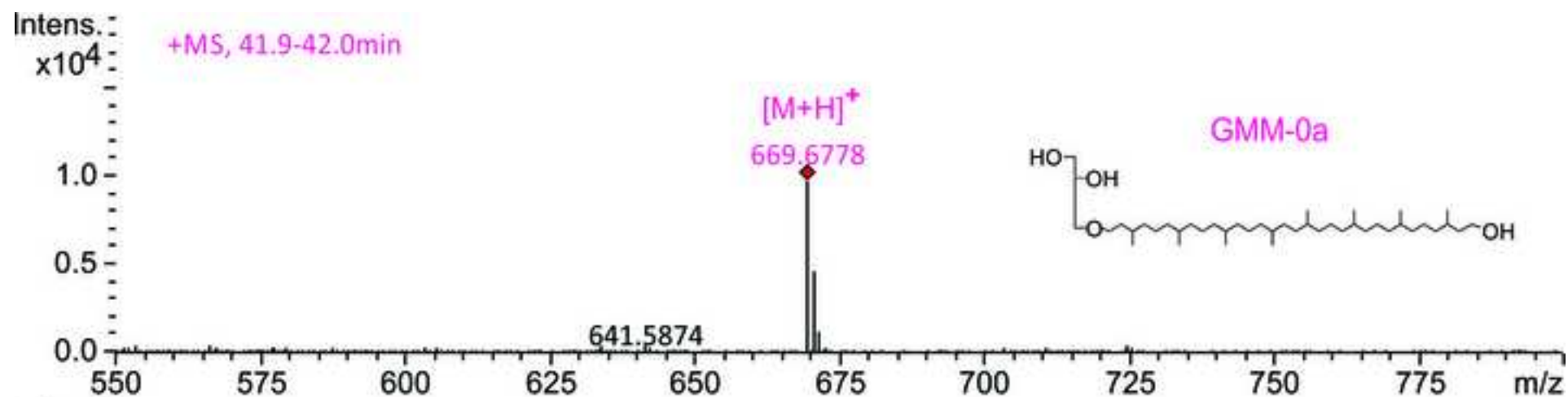


Figure
[Click here to download high resolution image](#)



Figure

[Click here to download high resolution image](#)

Figure

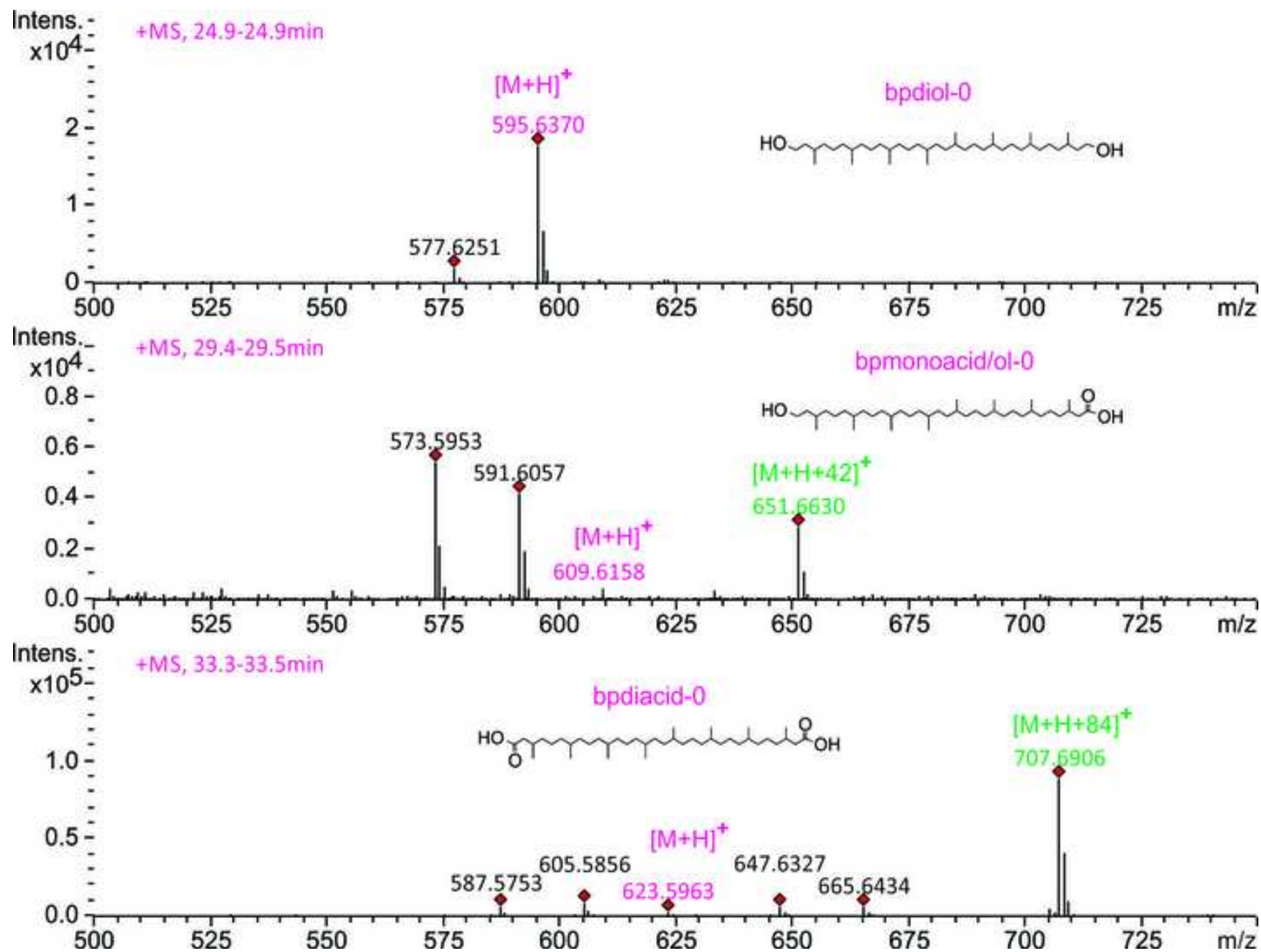
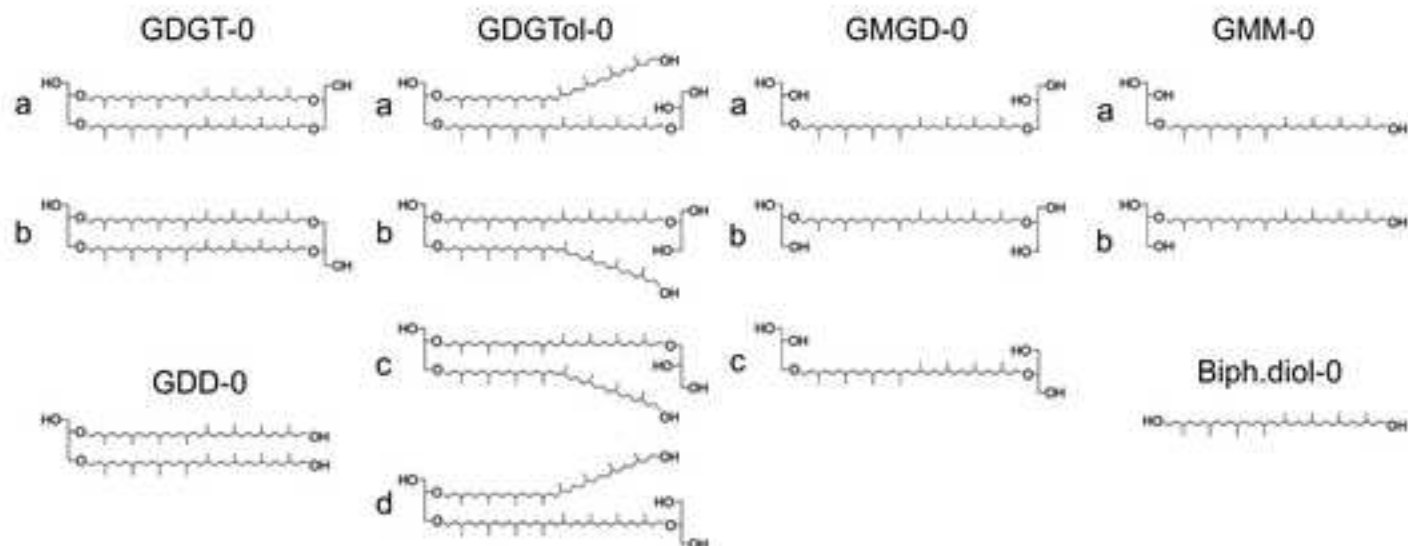
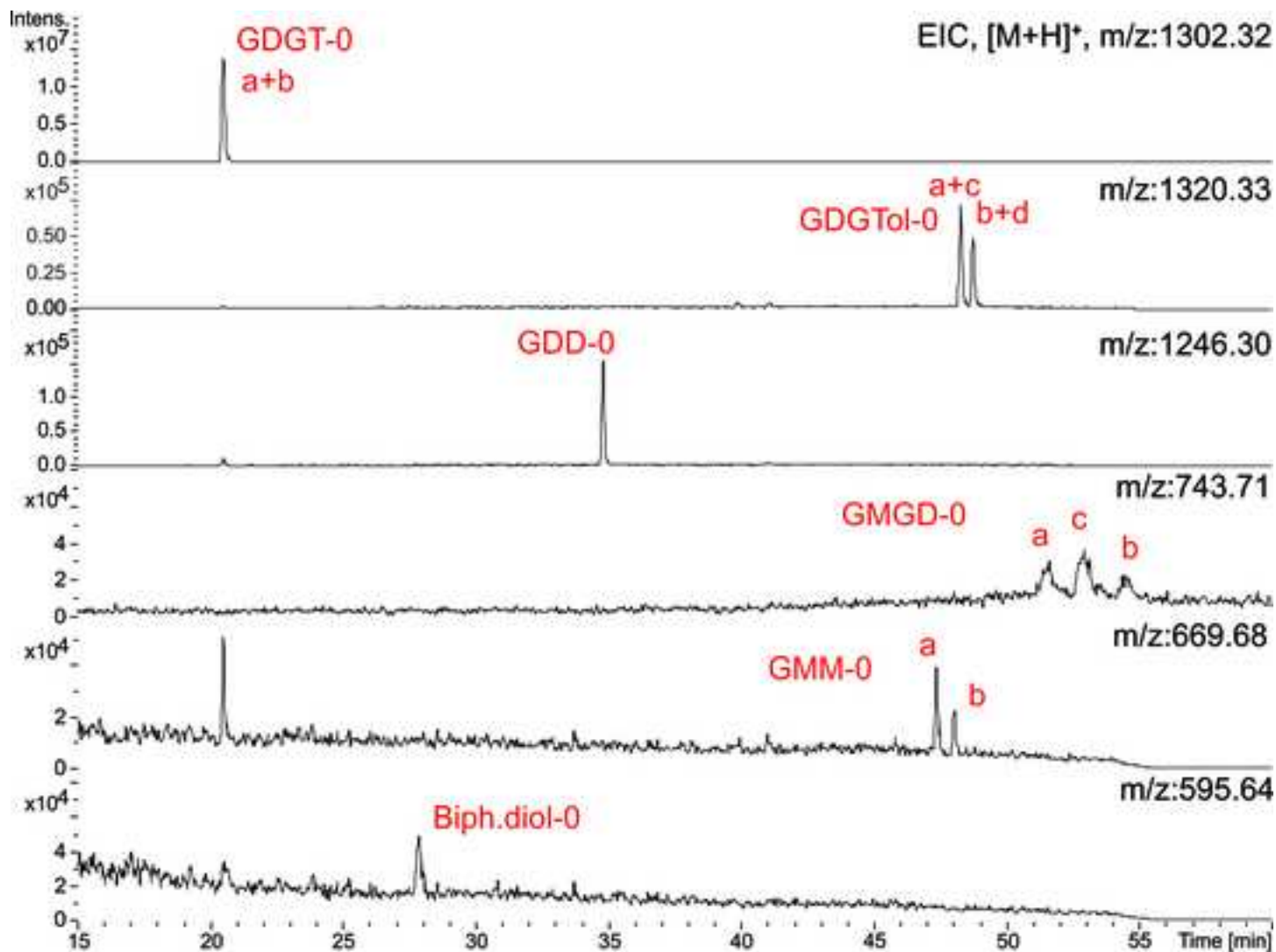
[Click here to download high resolution image](#)

Figure
[Click here to download high resolution image](#)



Figure

[Click here to download high resolution image](#)

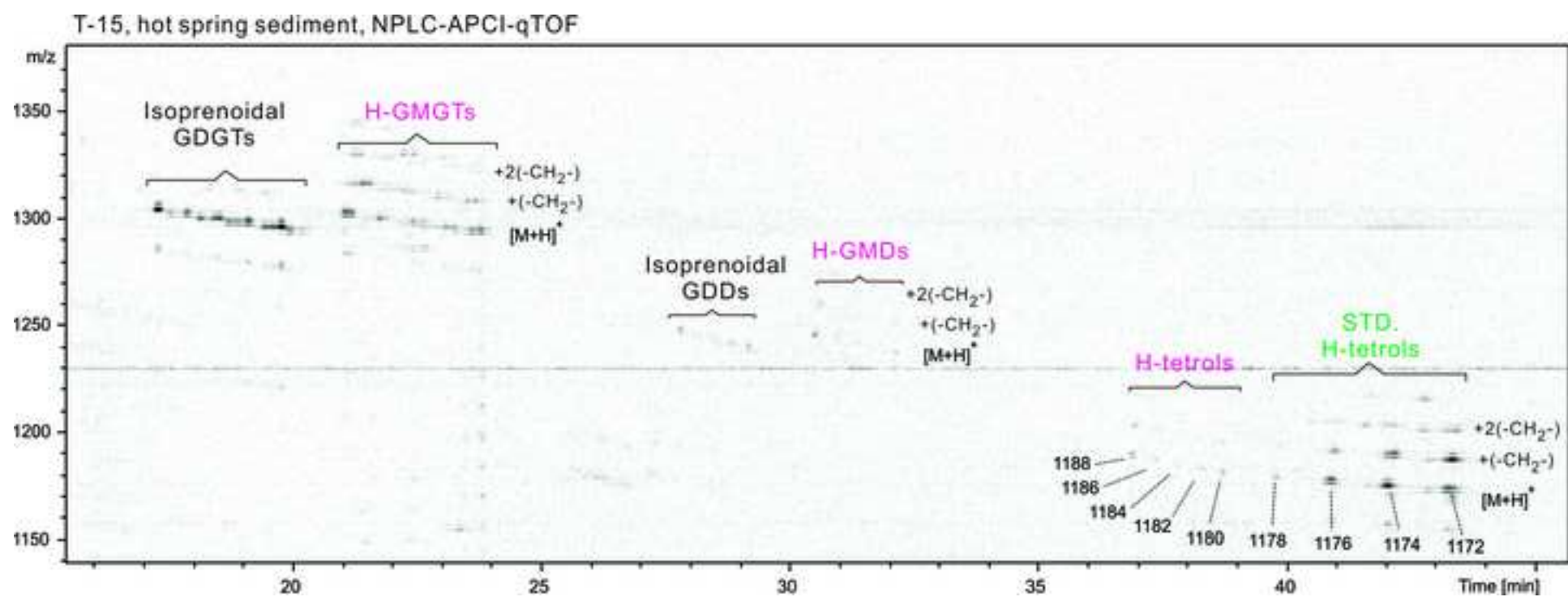


Figure
[Click here to download high resolution image](#)

Marmorito seep carbonate, NPLC-APCI-qTOF

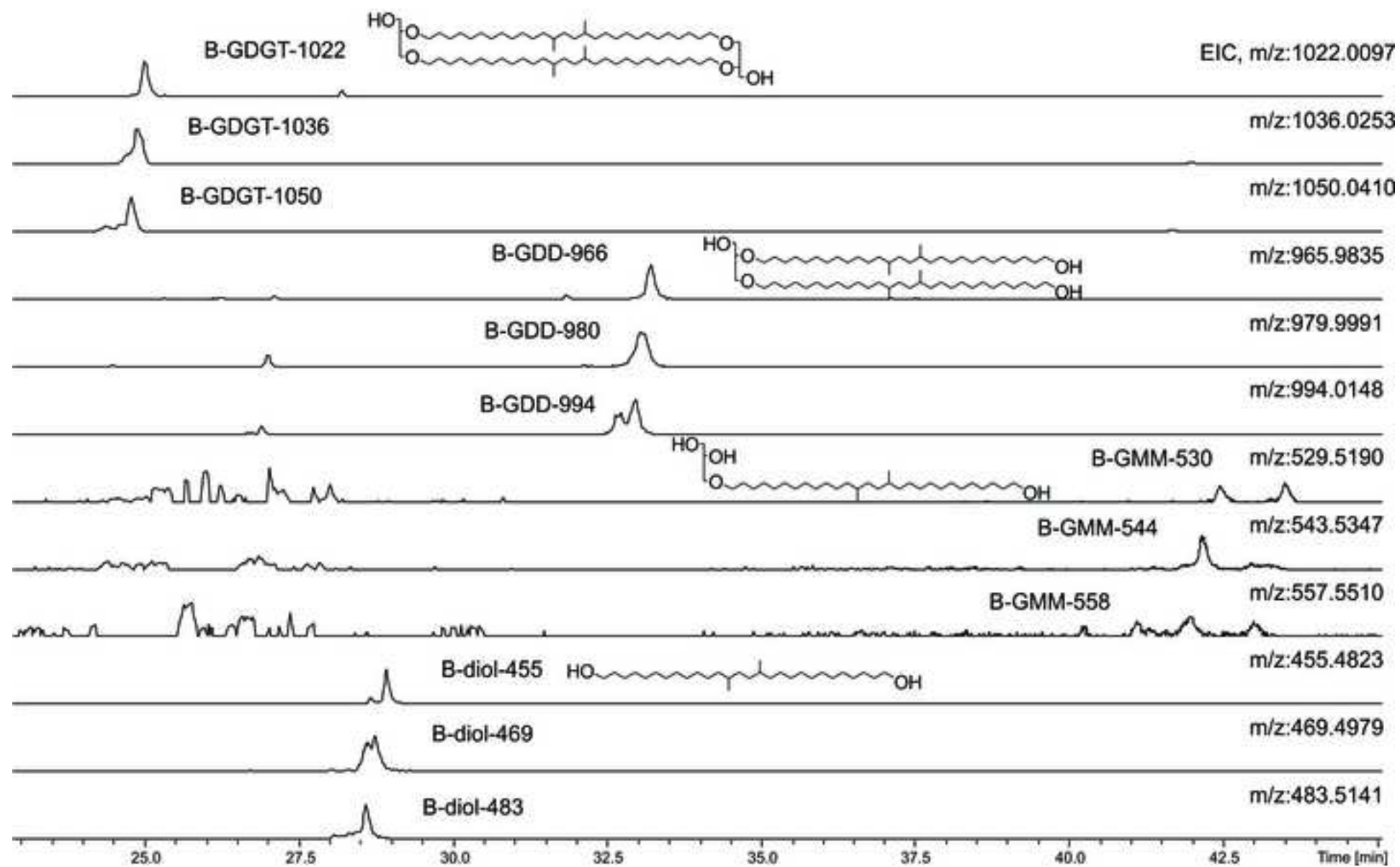


Figure
[Click here to download high resolution image](#)

Marmorito seep carbonate, NPLC-APCI-qTOF

